Regularized extended-hydrodynamic equations for a rarefied granular gas and the plane shock waves

M. H. Lakshminarayana Reddy and Meheboob Alam*
Jawaharlal Nehru Center for Advanced Scientific Research, Jakkur P.O., Bangalore 560064, India

(Received 29 November 2019; accepted 5 February 2020; published 6 April 2020)

The regularized versions of extended-hydrodynamic equations for a dilute granular gas, in terms of 10-, 13-, and 14-moments, are derived from the inelastic Boltzmann equation. The regularization is achieved by adding higher-order gradient terms that are obtained following a Chapman-Enskog-like gradient-expansion [H. Struchtrup, Stable transport equations for rarefied gases at high orders in the Knudsen number, Phys. Fluids, **16**, 3921 (2004)]. For both granular and molecular gases, the resulting moment equations are found to be free from the well-known finite Mach-number singularity (that occurs in the Riemann problem of planar shock waves) since the regularized gradient terms yield parabolic equations in contrast to the hyperbolic nature of original moment equations. In order to clarify the advantage of these regularized equations, the 10-moment model for the plane shock-wave problem is solved numerically for both molecular and granular gases; the calculated hydrodynamic profiles compare favorably with previous simulation results for molecular gases. For a granular gas, both regularized and nonregularized equations predict asymmetric density and temperature profiles, with the maxima of both density and temperature occurring within the shock layer, and the hydrodynamic fields are found to be smooth for the regularized equations for all Mach numbers studied. It is demonstrated that, unlike in the case of molecular gases, a "second" regularization of the regularized equations must be carried out in order to arrest the unbounded growth of density within the shock layer in a granular gas.

DOI: 10.1103/PhysRevFluids.5.044302

I. INTRODUCTION

Researchers from different areas have extensively studied the behavior of granular materials under various physical constraints over the last four decades [1–14]. Depending on the external forcing [15], the granular materials can (1) behave like a solid (such as in a sand-pile), (2) flow like a liquid (like in an hour-glass), and (3) act like a a gas (like in dust storms); the last two states fall under the category of "rapid" granular flows [16,17]. Rapid flows of granular materials occur in geophysical and other natural phenomena such as snow avalanches, rock and land slides, sand dunes, interstellar dust, planetary rings, etc. Under strong external driving, the grains move around randomly, which is reminiscent of the motion of atoms in a molecular gas except that the macroscopic particles collide inelastically, resulting in a loss of kinetic energy, and hence the fluidized mode of granules is termed as a "granular" or "inelastic" gas [18,19]. The driven granular gases are often found in the rarefied regime since the Knudsen number ($\mathrm{Kn} \geqslant 0.01$), the ratio of the mean-free path (λ) and the characteristic length scale (L) of the system, which characterizes the gas rarefaction, is large. At the macroscopic level, granular gases are frequently modelled by hydrodynamic-like equations [1–3,20–27] modified to account for inelastic dissipation.

*meheboob@jncasr.ac.in

One needs to develop accurate hydrodynamic models that can be used for the modeling of flows in the rarefied regime (Kn $\geqslant 0.01$): the standard hydrodynamic equations, namely, Euler and Navier-Stokes-Fourier equations, are inappropriate since the hypothesis of scale separation is violated in the rarefied regime. On the other hand, the rarefied gas flows are well described by the Boltzmann equation, which describes the evolution of the single-particle distribution function and the solution to the same via direct simulation Monte Carlo (DSMC) technique has been found to be useful in the rarefied regime, but this method is prohibitive with regard to computational requirements. From the viewpoint of continuum equations, modeling rarefied or nonequilibrium gas flows requires one to go beyond Navier-Stokes order by considering an extended set of hydrodynamic fields; the present work is based on the latter approach of Grad [28] to model granular gases.

In the "extended" hydrodynamic description [28,29], the problem of directly solving the Boltzmann equation is replaced by solving a system of balance equations for higher moments (of distribution function) beyond the standard set of five hydrodynamic fields (density, velocity, and temperature). In general it is assumed that the addition of more moments gives rise to a system of balance equations, which approximate nonequilibrium flows accurately [26,28–31]. The Chapman-Enskog method [32], based on a perturbation expansion in terms of the Knudsen number, is a well-known technique to derive "extended" hydrodynamic equations; this yields Euler equations at zeroth-order expansion, the equations of Navier-Stokes and Fourier at the first order, Burnett equations at the second order, super-Burnett equations at the third order, and so on [31–33]. Note that Burnett and super-Burnett equations are known to be unstable for the rest state with small-wavelength perturbations [34]. The second approach of obtaining a closed extended moment system is Grad's moment method [28,30], in which the distribution function is expanded in terms of Hermite polynomials in the components of the fluctuating velocity, with the Maxwellian distribution function (equilibrium distribution function) as weight function. Grad's method introduces an additional set of evolution equations for the stress tensor, heat flux, and higher-order moments of the distribution function. By truncating the Hermite polynomial expansion, one can obtain a closed system of moment equations up to the desired order of moments.

However, it is well known (see Appendix A) that the moment models formulated from Grad's moment method, when applied to stationary shock problem, suffer from a subshock formation for Mach numbers greater than a critical Mach number of the respective moment model. Regularization or parabolization is one method to obtain a smooth shock profile beyond the critical Mach number [35]. On the other hand, the regularization process changes the character of the hyperbolic system by adding some parabolic terms in the form of the higher-order gradient expressions. For example, in the original Grad's 10-moment system [28] the contribution from the third-order moments of the distribution function are set to zero, but if one follows the regularization procedure [31,35–37] for the 10-moment model, the expressions for higher-order moments like heat flux vector and the third-order traceless moment are found to be nonzero; the latter terms contain the second-order gradient of lower-order moments of the distribution function, which are responsible for changing the hyperbolic nature of the 10-moment system to parabolic and help to yield smooth shock profiles beyond the critical Mach number. For a different viewpoint and the related issues on "hyperbolic" regularization of Burnett equations that are free from the well-known short-wave instability [34], readers are referred to Refs. [38,39].

Returning to Grad-type models, Fig. 1 confirms that the predictions for the shock thickness [36,37] are accurate for higher-order models like R13 (regularized 13-moment model) over the Navier-Stokes-Fourier model, as the results from R13 model show a better agreement with the DSMC data. This motivates us to develop extended hydrodynamic models and their regularized versions to calculate the shock structures in rarefied granular gases. This forms the main objective of the current work: to derive regularized moment equations for inelastic hard spheres following the Chapman-Enskog-like "order-of-magnitude" method of Struchtrup [35]. Towards this goal, the regularized versions of 14-moment (R14), 13-moment (R13), and 10-moment (R10) equations are derived for a dilute granular gas, which forms the primary focus of this paper. In addition, to

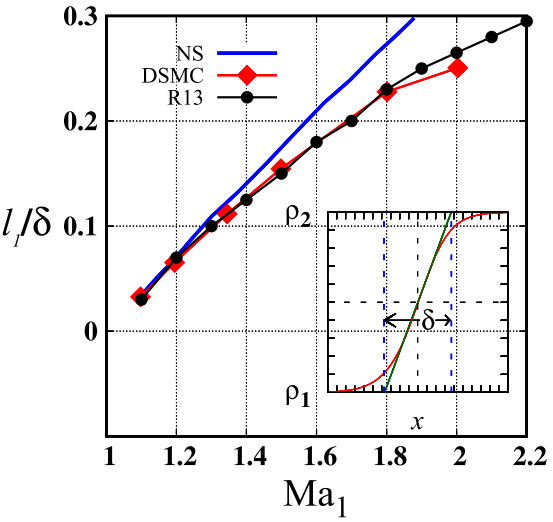

FIG. 1. Dimensionless inverse shock width (l_1/δ) versus upstream Mach number (Ma_1) for the stationary plane shock-wave problem for a hard-sphere gas. All data are extracted from Ref. [37]: NS and R13 refer to solutions from Navier-Stokes and "regularized" 13-moment equations, respectively; results from DSMC are also superimposed. The inset displays the variation of normalized density across the shock and the definition of shock width δ.

clarify the advantage of regularized moment equations, the R10 equations are subsequently solved to analyze the plane shock-wave problem for both molecular and granular gases.

This paper is organized as follows. In Sec. II a brief overview of the 14-moment equations for a granular gas is presented based on Grad's method [28]; Sec. II C is devoted to discussing the need for regularized moment equations, with reference to an analysis of the inviscid Burgers equation and its regularized counterpart. In Sec. III the regularized versions of 14-moment, 13-moment, and 10-moment equations are derived by following a Chapman-Enskog-like gradient expansion; furthermore, the granular Navier-Stokes-order equations are derived in Appendix B as a regularization of the corresponding Euler-level equations. The details of the formulation of the granular plane shock problem and Rankine-Hugoniot conditions for a granular gas are provided in Sec. IV. The influence of regularization in predicting a smooth shock solution beyond critical Mach number is judged in Sec. V, by applying the present R10 moment equations to the shock-wave problem in an ideal gas using the numerical scheme discussed in Appendix D. The derivation of Haff's law [3] from 10-moment and 14-moment models and their differences are discussed in Appendix E. In Sec. VI the early-time and long-time dynamics of granular shock-wave profiles are discussed; the need for a "second" regularization of regularized equations is critically analyzed. Finally, the conclusions are drawn based on current analysis and possible future work is suggested in Sec. VII.

II. A BRIEF OVERVIEW OF EXTENDED HYDRODYNAMIC EQUATIONS FOR GRANULAR GASES AND THE DISCONTINUOUS SHOCK SOLUTION

We consider a dilute granular gas of smooth, inelastic spheres of mass m and diameter d that interact via binary collisions. The state of the granular gas is described by the single-particle distribution function $f(\mathbf{r}, \mathbf{v}, t)$ whose evolution is governed by the Boltzmann equation, which, in the absence of external forces, reads

$$\frac{\partial f}{\partial t} + \mathbf{v} \cdot \frac{\partial f}{\partial \mathbf{r}} = d^2 \int_{g \cdot k > 0} \left[\frac{1}{\alpha^2} f(\mathbf{r}, \mathbf{v}_1'', t) f(\mathbf{r}, \mathbf{v}'', t) - f(\mathbf{r}, \mathbf{v}_1, t) f(\mathbf{r}, \mathbf{v}, t) \right] (g \cdot k) \, dk \, d\mathbf{v}_1, \quad (1)$$

where we have made use of the ansatz of *molecular chaos* [32,33]. The inelastic nature of collisions of macroscopic particles is characterized via $(g' \cdot k) = -\alpha(g \cdot k)$, where $g = (\mathbf{v}_1 - \mathbf{v})$ and $g' = (\mathbf{v}_1' - \mathbf{v}')$ denote the relative velocities of colliding particles before and after a collision, respectively, k is the unit contact vector pointing from the center of the particle denoted by index 1 to the center of the other particle without index, and $\alpha \in (0, 1)$ is the coefficient of restitution, with $\alpha = 1$ and 0 representing perfectly elastic and sticky collisions, respectively. In the following we provide a brief sketch of the derivation of extended hydrodynamic equations in terms of 14 moments, starting from the Boltzmann equation (1).

A. Extended hydrodynamic variables

The macroscopic/hydrodynamic field variables are obtained via a coarse-graining procedure over the distribution function $f(\mathbf{r}, \mathbf{v}, t)$,

$$\langle \psi(\mathbf{v}) \rangle = \int \psi(\mathbf{v}) f(\mathbf{r}, \mathbf{v}, t)\, d\mathbf{v}, \tag{2}$$

where $\psi(\mathbf{v})$ is a polynomial of the particle velocity $\mathbf{v}$. For example, to obtain the 13-moment theory of Grad [28], one has to take $\psi = m\{1, v_i, \frac{1}{3}C^2, C_{\langle i}C_{j\rangle}, \frac{1}{2}C^2 C_i\}$, which yields the relevant field variables for the 13-moment system:

$$\begin{aligned} &\rho = mn \text{ (mass density)}, \quad \rho\, u_i \text{ (momentum)}, \quad \theta \text{ (temperature)}, \\ &\sigma_{ij} \text{ (stress deviator)}, \quad q_i \text{ (heat flux)}, \end{aligned} \tag{3}$$

where $C = \mathbf{v} - \boldsymbol{u}$ is the peculiar velocity, n is the number density, and the angular brackets around subscripts, such as in $C_{\langle i}C_{j\rangle}$ and below, denote the deviatoric part of the respective tensor. In order to obtain the 14-moment system [40], an extra moment, namely, the fully contracted fourth-order moment,

$$\mathcal{R} = \langle m C^4 \rangle = \int m C^4 f(\mathbf{r}, \mathbf{v}, t)\, d\mathbf{v}, \tag{4}$$

is added, which is an important field variable for a granular gas [23–26]. Instead of $\mathcal{R}$ in Eq. (4), it is convenient to use its dimensionless nonequilibrium part, denoted by Δ, and defined via

$$\Delta = \frac{1}{15\,\rho\,\theta^2}(\mathcal{R} - \mathcal{R}^{\rm eq}) = \frac{1}{15\,\rho\,\theta^2} \int m C^4 (f - f^M)\, d\mathbf{v}, \tag{5}$$

as a separate field variable, where

$$f^M = \frac{n}{(2\pi\theta)^{\frac{3}{2}}} e^{-\frac{C^2}{2\theta}} \tag{6}$$

is the equilibrium distribution function. It is straightforward to verify that $\mathcal{R}^{\rm eq} = 15\rho\theta^2$, and the related details can be found in Kremer and Marques [40].

B. 14-moment equations

The hydrodynamic/moment equations are obtained by multiplying the Boltzmann equation (1) by $\psi(\mathbf{v})$ and integrating the resulting equation over the velocity space. With an appropriate choice of $\psi(\mathbf{v})$, the extended hydrodynamic system for 14 moments $(\rho, \rho\, u_i, \theta, \sigma_{ij}, q_i, \Delta)$ can be written as

$$\frac{\partial \rho}{\partial t} + \frac{\partial(\rho\, u_i)}{\partial x_i} = 0, \tag{7a}$$

$$\frac{\partial(\rho\, u_i)}{\partial t} + \frac{\partial(\rho\, u_i\, u_j)}{\partial x_j} + \frac{\partial p}{\partial x_i} + \frac{\partial \sigma_{ij}}{\partial x_j} = 0, \tag{7b}$$

$$\rho\left(\frac{\partial\theta}{\partial t}+u_i\frac{\partial\theta}{\partial x_i}\right)+\frac{2}{3}\left(\rho\,\theta\frac{\partial u_i}{\partial x_i}+\sigma_{ij}\frac{\partial u_i}{\partial x_j}+\frac{\partial q_i}{\partial x_i}\right)=-\mathcal{D}, \tag{7c}$$

$$\frac{\partial\sigma_{ij}}{\partial t}+\frac{\partial(\sigma_{ij}\,u_k)}{\partial x_k}+\frac{4}{5}\frac{\partial q_{\langle i}}{\partial x_{j\rangle}}+2\,p\,\frac{\partial u_{\langle i}}{\partial x_{j\rangle}}+2\,\sigma_{k\langle i}\frac{\partial u_{j\rangle}}{\partial x_k}+\underline{\frac{\partial\mathcal{Q}_{ijk}}{\partial x_k}}=\sigma^s_{ij}, \tag{7d}$$

$$\begin{aligned}&\frac{\partial q_i}{\partial t}+\frac{\partial(q_i\,u_j)}{\partial x_j}-\frac{5}{2}\,\theta\left(\rho\,\frac{\partial\theta}{\partial x_i}+\theta\,\frac{\partial\rho}{\partial x_i}+\frac{\partial\sigma_{ij}}{\partial x_j}\right)-\frac{\sigma_{ij}}{\rho}\left(\rho\,\frac{\partial\theta}{\partial x_j}+\theta\,\frac{\partial\rho}{\partial x_j}+\frac{\partial\sigma_{jk}}{\partial x_k}\right)\\&\quad+\frac{7}{5}\,q_j\frac{\partial u_i}{\partial x_j}+\frac{2}{5}\,q_i\frac{\partial u_j}{\partial x_j}+\frac{2}{5}\,q_k\frac{\partial u_k}{\partial x_i}+\underline{\frac{1}{2}\frac{\partial\mathcal{R}_{ij}}{\partial x_j}+\frac{1}{6}\frac{\partial\mathcal{R}}{\partial x_i}+\mathcal{Q}_{ijk}\frac{\partial u_j}{\partial x_k}}=q^s_i,\end{aligned} \tag{7e}$$

$$\begin{aligned}&15\,\rho\,\theta^2\left(\frac{\partial\Delta}{\partial t}+u_i\,\frac{\partial\Delta}{\partial x_i}\right)-20\,(1+\Delta)\,\theta\left(\frac{\partial q_i}{\partial x_i}+\sigma_{ij}\frac{\partial u_i}{\partial x_j}\right)-8\,q_i\,\frac{\partial\theta}{\partial x_i}\\&\quad-\frac{8}{\rho}\,q_i\left(\frac{\partial\sigma_{ij}}{\partial x_j}+\theta\,\frac{\partial\rho}{\partial x_i}\right)+\underline{\frac{\partial\mathcal{S}_i}{\partial x_i}+4\,\mathcal{R}_{ij}\,\frac{\partial u_i}{\partial x_j}}=\Delta^s,\end{aligned} \tag{7f}$$

where, as stated above, the deviatoric part of any tensor field is denoted by the angular brackets over its subscripts; for example,

$$\frac{\partial u_{\langle i}}{\partial x_{j\rangle}}=\frac{1}{2}\left(\frac{\partial u_i}{\partial x_j}+\frac{\partial u_i}{\partial x_j}\right)-\frac{1}{3}(\boldsymbol{\nabla}\cdot u)I_{ij}, \tag{8}$$

is traceless and I_{ij} is the identity tensor. The underlined terms on the left-hand side in Eqs. (7d)–(7f) are of "higher order" (than the order of the field variable in the respective equation) as given by

$$\left.\begin{aligned}\mathcal{Q}_{ijk}&=\int m\,C_{\langle i}C_jC_{k\rangle}f(\mathbf{r},\mathbf{v},t)\,d\mathbf{v}\\\mathcal{R}_{ij}&=\int m\,C^2C_{\langle i}C_{j\rangle}f(\mathbf{r},\mathbf{v},t)\,d\mathbf{v}\\\mathcal{S}_i&=\int m\,C^2C^2C_if(\mathbf{r},\mathbf{v},t)\,d\mathbf{v}\end{aligned}\right\}, \tag{9}$$

where $\mathcal{Q}_{ijk}$ and $\mathcal{R}_{ij}$ are traceless tensors of third and second rank, respectively. The source terms on the right-hand side of Eqs. (7c)–(7f) are given by

$$\mathcal{D}=\frac{m\,d^2\,(1-\alpha^2)}{12}\int_{\boldsymbol{g}\cdot\boldsymbol{k}>0}(\boldsymbol{g}\cdot\boldsymbol{k})^2\,d\boldsymbol{\Omega}, \tag{10a}$$

$$\sigma^s_{ij}=\frac{md^2}{2}\int_{\boldsymbol{g}\cdot\boldsymbol{k}>0}(C'_{\langle i}C'_{j\rangle}+C'_{1_{\langle i}}C'_{1_{j\rangle}}-C_{\langle i}C_{j\rangle}-C_{1_{\langle i}}C_{1_{j\rangle}})\,d\boldsymbol{\Omega}, \tag{10b}$$

$$q^s_i=\frac{md^2}{4}\int_{\boldsymbol{g}\cdot\boldsymbol{k}>0}\left(C'^2C'_i+C'^2_1C'_{1_i}-C^2\,C_i-C^2_1\,C_{1_i}\right)d\boldsymbol{\Omega}, \tag{10c}$$

$$\Delta^s=30\,(1+\Delta)\,\theta\mathcal{D}+\frac{md^2}{2}\int\left(C'^4+C'^4_1-C^4-C^4_1\right)d\boldsymbol{\Omega}, \tag{10d}$$

where

$$d\boldsymbol{\Omega}=(\boldsymbol{g}\cdot\boldsymbol{k})\,f(\mathbf{r}_1,\mathbf{v}_1,t)\,f(\mathbf{r},\mathbf{v},t)\,d\boldsymbol{k}\,d\mathbf{v}_1\,d\mathbf{v}. \tag{11}$$

Equations (7a) and (7b) represent the conservation laws for mass and momentum, respectively, while Eqs. (7c), (7d), (7e), and (7f) represent the balance equations for the fluctuation energy, the deviatoric part of the pressure tensor, the heat-flux vector, and the dimensionless nonequilibrium part of fourth-order contracted moment, respectively. Note that Eqs. (7d)–(7f) do not form a closed set since they contain additional moments, $\mathcal{Q}_{ijk}$, $\mathcal{R}_{ij}$, and $\mathcal{S}_i$, of higher order as defined in Eq. (9), which in turn require knowledge about the single-particle distribution function.

1. Distribution function for 14 moments

In terms of the field variables under consideration for the 14-moment system, the nonequilibrium distribution function is obtained from a Hermite expansion [28] around the Maxwellian distribution function:

$$f(\mathbf{r}, \mathbf{v}, t) = \frac{n}{(2\pi\theta)^{\frac{3}{2}}} e^{-\frac{C^2}{2\theta}} \left(\sum_{i=0}^{M} a^{(i)} \mathcal{H}^{(i)} \right), \tag{12}$$

where $\mathcal{H}^{(i)}$ denote ith-order Hermite polynomials and $a^{(i)}$ are the expansion coefficients which are related to the moments of the distribution function. The number of terms M retained in Eq. (12) is dictated by physical considerations; it is often argued [28] that the macroscopic state of a gas can be characterized by the 10, 13, and 14 basic field variables for 10-moment, 13-moment, and 14-moment systems, respectively. The resulting distribution function for 14-moment theory reads

$$f|_{14} = f^M \left[1 + \frac{\sigma_{ij}}{2\rho\theta^2} C_i C_j + \underline{\frac{q_i}{5\rho\theta^3} (C^2 - 5\theta) C_i} + \underline{\left(\frac{C^4 - 10C^2\theta + 15\theta^2}{8\theta^2} \right) \Delta} \right]. \tag{13}$$

Deleting the two underlined terms and the last underlined term in Eq. (13) results in the distribution function for the 10- and 13-moment theories, respectively, for which the field variables are $(\rho, u_i, \theta, \sigma_{ij})$ and $(\rho, u_i, \theta, \sigma_{ij}, q_i)$. We shall return to discuss the 13- and 10-moment systems in Secs. III C and III D, respectively.

2. Evaluation of source/production terms

Using the 14-moment distribution function, Eq. (13), the higher-order moments, Eq. (9), are evaluated as

$$\mathcal{Q}_{ijk|14} = 0, \quad \mathcal{R}_{ij|14} = 7\,\theta\,\sigma_{ij}, \quad \mathcal{S}_{i|14} = 28\,\theta\,q_i, \tag{14}$$

with the subscript 14 on the above quantities denoting that Eq. (14) holds for the 14-moment theory. The collisional source terms in Eqs. (10a)–(10d) are evaluated as [40]

$$\mathcal{D} = \frac{4}{3\,\tau_r} (1 - \alpha^2) \left[1 + \frac{3\,\Delta}{16} + \frac{9\Delta^2}{1024} \right] \rho\theta, \tag{15a}$$

$$\sigma_{ij}^s = -\frac{4}{5\,\tau_r} (1 + \alpha)(3 - \alpha) \left[1 - \frac{\Delta}{32} \right] \sigma_{ij}, \tag{15b}$$

$$q_i^s = -\frac{1}{15\,\tau_r} (1 + \alpha) \left[49 - 33\,\alpha + (19 - 3\,\alpha) \frac{\Delta}{32} \right] q_i, \tag{15c}$$

$$\Delta^s = \frac{4}{\tau_r} (1 + \alpha) \left\{ (1 - \alpha)(1 - 2\,\alpha^2) - [30\,\alpha^2 (1 - \alpha) - 17\,\alpha + 81] \frac{\Delta}{16} \right.$$
$$\left. + [30\alpha^2(1 - \alpha) - 2001\alpha + 1873] \frac{\Delta^2}{1024} \right\} \rho\theta^2. \tag{15d}$$

Note that we have retained quadratic terms in Δ to evaluate both $\mathcal{D}$ and Δ^s; on the other hand, to evaluate σ_{ij}^s and q_i^s, in addition to the linear terms in σ_{ij} and q_i, the quadratic terms in the form of the product of Δ with σ_{ij} and q_i are retained. In the above equations (15a)–(15d), τ_r is a relaxation time given by

$$\tau_r = \frac{m}{\rho\, d^2 \sqrt{\pi\,\theta}}. \tag{16}$$

Insertion of Eqs. (14)–(15d) into the balance equations (7a)–(7f) yields a closed set of 14-moment equations for a dilute granular gas; this is called the "14-moment" model. For both "dilute" granular and molecular gases, it is a straightforward exercise (with the help from computer algebra) to evaluate and include nonlinear terms of arbitrary order in the production terms in Eqs. (15a)–(15d) that we would not consider in this work.

C. Discontinuous shock solution and the need for regularization

Unlike the Navier-Stokes (NS) equations that admit continuous shock profiles for the Cauchy problem, the higher-order moment system (such as 10-, 13-, and 14-moment equations) is symmetric hyperbolic [29] and develops discontinuous stationary shocks beyond a minimum value of the Mach number. The analysis of the Riemann problem of stationary shock waves in Appendix A indicates that the critical Mach numbers for 10-, 13-, and 14-moment models are $\mathrm{Ma}_{\mathrm{cr}}|_{10} = 1.34$, $\mathrm{Ma}_{\mathrm{cr}}|_{13} = 1.65$, and $\mathrm{Ma}_{\mathrm{cr}}|_{14} = 1.763$, respectively. This implies that the range of Mach numbers over which smooth shock solution exists increases with increasing number of field variables [41]. Before remedying this problem of discontinuous shock solutions admitted by higher-order hydrodynamic equations, we briefly discuss the regularization of the inviscid Burgers equation via viscosity in the following section.

1. Inviscid Burgers equation and its regularization

The inviscid Burgers equation is the simplest nonlinear equation that admits discontinuous solutions for the Cauchy problem even with arbitrary smooth initial data [42]. This is a nonlinear "hyperbolic" conservation equation,

$$\frac{\partial u}{\partial t} + u\,\frac{\partial u}{\partial x} = 0, \tag{17}$$

whose solution $u(x,t)$ represents nonlinear waves for which the propagation speed of a point on the wave profile is equal to its amplitude at that point. The latter property is responsible for the steepening of the wave $u(x,t)$ with time, even if the initial wave profile $[u(x,0) = \phi(x)]$ is a C_0^∞ function. It is straightforward to verify that the slope of $u(x,t)$ becomes ∞ at a critical time beyond which the wave profile becomes multivalued. Immediately after the critical time, a single-valued solution can be constructed satisfying the integral version of Eq. (17), called the weak solution [42], that includes a discontinuity in the wave profile $u(x,t)$. This discontinuous solution or the shock satisfies the entropy condition and can be constructed via Maxwell's equal-area rule; the formation of shock can also be explained from the geometry of the characteristic curves of Eq. (17); for details we refer to Refs. [42,43].

Now we consider the equation originally considered by Bateman [44] and studied extensively by Burgers [45] which includes a diffusive term to Eq. (17):

$$\frac{\partial u}{\partial t} + u\,\frac{\partial u}{\partial x} = \nu\,\frac{\partial^2 u}{\partial x^2}, \tag{18}$$

where ν is the kinematic viscosity. Equation (18) is called the viscous Burgers equation, and this is the simplest model equation which combines the nonlinear and viscous effects. Due to the presence of the nonlinear convective term and the viscosity term, Eq. (18) can be considered as a simplified form of the one-dimensional Navier-Stokes equation without pressure terms. In any case, the steady-state solutions of the viscous Burgers equation (18) for the piecewise constant initial data

$$u(x,0) = \begin{cases} u_l = 1 & \text{if } x < 0 \\ u_r = 0 & \text{if } x > 0 \end{cases} \tag{19}$$

are shown in Fig. 2 for $\nu = 0.025$, 0.05, and 0.1, along with its limiting discontinuous solution $\nu \to 0$. If the viscosity ν is very small and the initial data are smooth, the viscous term $\nu\,(\partial^2 u/\partial x^2)$ is negligible as compared to the other terms at $t \ll t_{\mathrm{cr}}$, and hence the solutions to both equations (17)

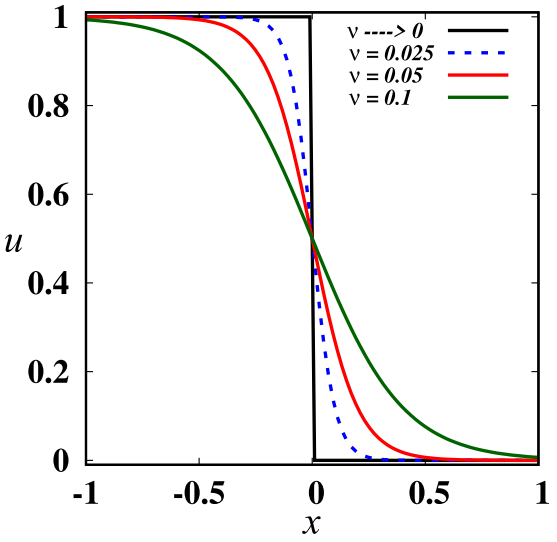

FIG. 2. Steady-state profiles of the solutions of the viscous Burgers equation (18) for the initial data given in Eq. (19), with ν equal to 0.025, 0.05, 0.1 and the limit of $\nu \to 0$.

and (18) would be nearly identical. However, as the wave starts to overturn (at $t \geqslant t_{\rm cr}$), the second derivative term $(\partial^2 u/\partial x^2)$ grows faster than $\partial u/\partial x$; hence the term $\nu\,(\partial^2 u/\partial x^2)$ begins to play a role comparable to the nonlinear term. The dominance of the viscous term over the nonlinear term keeps the solution smooth at all times, preventing the overturning of the wave profile that occurs for the inviscid Burger equation. Therefore, one can recognize the viscous Burgers equation (18) as a regularized version of the inviscid Burgers equation (17) since it admits continuous solutions for any $\nu > 0$. The above arguments can be seamlessly carried over to the Navier-Stokes equations as a "regularized" version of Euler equations; see Appendix B.

2. Present work

As stated in Sec. I, the first goal of this paper is to derive a set of 14-moment equations for a granular gas which admits continuous shock solutions beyond its critical Mach number (i.e. at $\mathrm{Ma} > \mathrm{Ma}_{\rm cr} \sim 1.763$). Towards this goal, we follow the order-of-magnitude method of Ref. [35] as discussed briefly in Sec. III A. It is shown in Sec. III B that the resulting equations have additional higher-order gradient terms that regularize the original 14-moment theory [Eqs. (7a)–(7f)]. For a granular gas, we shall further demonstrate that the standard regularized equations must be "reregularized" (Sec. VI C) to avoid another singularity in the density field as discovered recently [11] for the same granular shock-wave problem using the Navier-Stokes model.

III. REGULARIZATION OF EXTENDED-HYDRODYNAMIC EQUATIONS FOR A GRANULAR GAS

A. An overview of order-of-magnitude method

The order-of-magnitude method, introduced by Struchtrup [35], follows a Chapman-Enskog-like expansion in terms of higher-order field variables and is motivated from the "consistent-order extended thermodynamics" of Müller *et al.* [41] that follows the well-known Maxwellian iteration procedure [46]. This method consists of three basic steps [31,35]:

(1) Finding the order of magnitude λ of different moments. The main aim of this step is to check the order of magnitude of moments in powers of a small parameter (ε, say, the Knudsen number).

More specifically, a higher-order or nonconserved moment ψ is expanded in powers of ε as

$$\psi = \psi_0 + \varepsilon\,\psi_1 + \varepsilon^2\,\psi_2 + \cdots . \tag{20}$$

The above expansion is similar to the Chapman-Enskog expansion, which is applied on the distribution function. In this method the primary focus is to determine the leading order of ψ, unlike in the Chapman-Enskog expansion where we compute ψ_i for $i = 0, 1, 2, \ldots$. The leading order of a moment ψ is obtained by inserting the above ansatz (20) into the system of moment equations. If $\psi_i = 0$ for all $i < \lambda$, then a moment ψ is said to be of leading order λ. The order of magnitude of a moment ψ is nothing but the leading order of that moment.

(2) Construction of a moment set with a minimum number of moments at order λ.

(3) Last, the removal of terms in all equations that would lead to contributions of orders $\lambda > \lambda_0$ in the balance laws. The latter follows from the definition of the order of accuracy λ_0.

The above procedure is discussed in Appendix B, which illustrates how to obtain the Euler and Navier-Stokes-Fourier equations at zeroth and first order, respectively; at second order this yields the well-known 13-moment equations of Grad [28].

B. Derivation of regularized 14-moment (R14) equations

To regularize the 14-moment equations (7a)–(7f), we introduce the deviations of $\mathcal{Q}_{ijk}, \mathcal{R}_{ij}$, and $\mathcal{S}_i$ from their values obtained from the 14-moment distribution function, Eq. (13), as defined by

$$\left.\begin{aligned} \widetilde{\mathcal{Q}}_{ijk} &\equiv \mathcal{Q}_{ijk} - \mathcal{Q}_{ijk|_{14}} = \mathcal{Q}_{ijk} \\ \widetilde{\mathcal{R}}_{ij} &\equiv \mathcal{R}_{ij} - \mathcal{R}_{ij|_{14}} = \mathcal{R}_{ij} - 7\,\theta\,\sigma_{ij} \\ \widetilde{\mathcal{S}}_i &\equiv \mathcal{S}_i - \mathcal{S}_{i|_{14}} = \mathcal{S}_i - 28\,\theta\,q_i \end{aligned}\right\}, \tag{21}$$

such that $\widetilde{\mathcal{Q}}_{ijk} = \widetilde{\mathcal{R}}_{ij} = \widetilde{\mathcal{S}}_i = 0$ for the 14-moment distribution function f_{14}.

In order to compute nonzero approximations for the deviation quantities in Eq. (21), the balance equations for $\mathcal{Q}_{ijk}, \mathcal{R}_{ij}$, and $\mathcal{S}_i$ are constructed from the Boltzmann equation:

$$\begin{aligned} &\frac{\partial \mathcal{Q}_{ijk}}{\partial t} + \frac{\partial(\mathcal{Q}_{ijk}\,u_l)}{\partial x_l} + \frac{\partial \mathcal{R}_{ijkl}}{\partial x_l} + \frac{3}{7}\,\frac{\partial \mathcal{R}_{\langle ij}}{\partial x_{k\rangle}} - \frac{3}{\rho}\,\sigma_{\langle ij}\,\frac{\partial p}{\partial x_{k\rangle}} - \frac{3}{\rho}\,\sigma_{\langle ij}\,\frac{\partial \sigma_{k\rangle l}}{\partial x_l} \\ &\quad + 3\,\mathcal{Q}_{l\langle ij}\,\frac{\partial u_{k\rangle}}{\partial x_l} + \frac{12}{5}\,q_{\langle i}\,\frac{\partial u_{k\rangle}}{\partial x_j} = \mathcal{Q}^s_{ijk}, \end{aligned} \tag{22a}$$

$$\begin{aligned} &\frac{\partial \mathcal{R}_{ij}}{\partial t} + \frac{\partial(\mathcal{R}_{ij}\,u_k)}{\partial x_k} + \frac{\partial \mathcal{N}_{ijk}}{\partial x_k} + \frac{2}{5}\,\frac{\partial \mathcal{S}_{\langle i}}{\partial x_{j\rangle}} + 2\,\mathcal{R}_{ijkl}\,\frac{\partial u_l}{\partial x_k} + \frac{14}{15}\,\mathcal{R}\,\frac{\partial u_{\langle i}}{\partial x_{j\rangle}} + 2\,\mathcal{R}_{k\langle i}\,\frac{\partial u_{j\rangle}}{\partial x_k} \\ &\quad + \frac{4}{5}\,\mathcal{R}_{k\langle i}\,\frac{\partial u_k}{\partial x_{j\rangle}} + \frac{6}{7}\,\mathcal{R}_{\langle ij}\,\frac{\partial u_{k\rangle}}{\partial x_k} - \frac{2}{\rho}\,\mathcal{Q}_{ijk}\,\frac{\partial p_{kl}}{\partial x_l} - \frac{28}{5\,\rho}\,q_{\langle i}\,\frac{\partial p_{j\rangle k}}{\partial x_k} = \mathcal{R}^s_{ij}, \end{aligned} \tag{22b}$$

$$\begin{aligned} &\frac{\partial \mathcal{S}_i}{\partial t} + \frac{\partial(\mathcal{S}_i\,u_j)}{\partial x_j} + \frac{\partial \mathcal{M}^{(6)}_{ij}}{\partial x_j} + 4\,\mathcal{N}_{ijk}\,\frac{\partial u_k}{\partial x_j} - \frac{4}{\rho}\,\mathcal{R}_{ij}\,\frac{\partial p_{jk}}{\partial x_k} - \frac{7}{3}\,\frac{\mathcal{R}}{\rho}\,\frac{\partial p_{ij}}{\partial x_j} \\ &\quad + \frac{4}{5}\left(\mathcal{S}_i\,\frac{\partial u_j}{\partial x_j} + \mathcal{S}_j\,\frac{\partial u_j}{\partial x_i}\right) + \frac{9}{5}\,\mathcal{S}_j\,\frac{\partial u_i}{\partial x_j} = \mathcal{S}^s_i. \end{aligned} \tag{22c}$$

The source terms in Eqs. (22a)–(22c) are defined as

$$\mathcal{Q}^s_{ijk} = \frac{md^2}{2}\int_{\boldsymbol{g}\cdot\boldsymbol{k}>0}\left(C'_{\langle i}C'_jC'_{k\rangle} + C'_{1_{\langle i}}C'_{1_j}C'_{1_{k\rangle}} - C_{\langle i}C_jC_{k\rangle} - C_{1_{\langle i}}C_{1_j}C_{1_{k\rangle}}\right)d\boldsymbol{\Omega}, \tag{23a}$$

$$\mathcal{R}^s_{ij} = \frac{md^2}{2}\int_{\boldsymbol{g}\cdot\boldsymbol{k}>0}\left(C'^2C'_{\langle i}C'_{j\rangle} + C'^2_1C'_{1_{\langle i}}C'_{1_{j\rangle}} - C^2C_{\langle i}C_{j\rangle} - C_1^2C_{1_{\langle i}}C_{1_{j\rangle}}\right)d\boldsymbol{\Omega}, \tag{23b}$$

$$\mathcal{S}^s_i = \frac{md^2}{2}\int_{\boldsymbol{g}\cdot\boldsymbol{k}>0}\left(C'^2C'^2C'_i + C'^2_1C'^2_1C'_{1_i} - C^2\,C^2\,C_i - C_1^2C_1^2\,C_{1_i}\right)d\boldsymbol{\Omega}, \tag{23c}$$

where $d\boldsymbol{\Omega}$ is defined in Eq. (11). The fourth-, fifth-, and sixth-order moments in Eqs. (22a)–(22c) are defined as

$$\left.\begin{aligned}\mathcal{R}_{ijkl} &= \int m\,C_{\langle i}C_jC_kC_{l\rangle}f(\mathbf{r},\mathbf{v},t)\,d\mathbf{v}\\ \mathcal{N}_{ijk} &= \int m\,C^2C_{\langle i}C_jC_{k\rangle}f(\mathbf{r},\mathbf{v},t)\,d\mathbf{v}\\ \mathcal{M}^{(6)}_{ij} &= \int m\,C^2C^2C_iC_jf(\mathbf{r},\mathbf{v},t)\,d\mathbf{v}\end{aligned}\right\}, \tag{24}$$

respectively, where $\mathcal{R}_{ijkl}$ and $\mathcal{N}_{ijk}$ are traceless tensors of fourth and third rank, respectively.

1. Procedure to calculate regularized terms for 14-moment theory

To find the nonzero contributions of $\widetilde{\mathcal{Q}}_{ijk}$, $\widetilde{\mathcal{R}}_{ij}$, and $\widetilde{\mathcal{S}}_i$ [see Eq. (21)], one has to consider linear contributions in terms of $\widetilde{\mathcal{Q}}_{ijk}$, $\widetilde{\mathcal{R}}_{ij}$, and $\widetilde{\mathcal{S}}_i$ when evaluating the above source terms. To determine the source terms, one must consider a distribution function which contains the moments under consideration, $\widetilde{\mathcal{Q}}_{ijk}$, $\widetilde{\mathcal{R}}_{ij}$, and $\widetilde{\mathcal{S}}_i$, for the regularization process. This requirement is satisfied by the fifth-order approximation for the distribution function [47]

$$\begin{aligned}f = f^M\Bigg[1 + \frac{\sigma_{ij}}{2\,\rho\,\theta^2}C_iC_j + \frac{q_i}{5\,\rho\,\theta^3}(C^2-5\,\theta)C_i + \left(\frac{C^4-10\,C^2\,\theta+15\,\theta^2}{8\,\theta^2}\right)\Delta\\ + \underline{\frac{\mathcal{Q}_{ijk}}{6\,\rho\,\theta^3}C_iC_jC_k} + \underline{\frac{(\mathcal{R}_{ij}-7\,\theta\,\sigma_{ij})}{28\,\rho\,\theta^4}(C^2-7\,\theta)C_iC_j}\\ + \underline{\frac{(\mathcal{S}_i-28\,\theta\,q_i)}{280\,\rho\,\theta^5}(C^4-14\,C^2\theta+35\,\theta^2)C_i}\Bigg],\end{aligned} \tag{25}$$

where three underlined terms (proportional to $\widetilde{\mathcal{Q}}_{ijk}$, $\widetilde{\mathcal{R}}_{ij}$, and $\widetilde{\mathcal{S}}_i$) are new in comparison to the distribution function in Eq. (13) that holds for a 14-moment system. It is straightforward to verify that Eq. (25) generates a system of 29-moment equations.

Employing Eq. (25), the source terms in Eqs. (23a)–(23c) have been evaluated which are linear in $\widetilde{\mathcal{Q}}_{ijk}$, $\widetilde{\mathcal{R}}_{ij}$, and $\widetilde{\mathcal{S}}_i$, respectively, as given by

$$\mathcal{Q}^s_{ijk} = -\frac{A_1}{\tau_r}\widetilde{\mathcal{Q}}_{ijk}, \quad \mathcal{R}^s_{ij} = -\frac{A_2}{\tau_r}\widetilde{\mathcal{R}}_{ij}, \quad \mathcal{S}^s_i = -\frac{A_3}{\tau_r}\widetilde{\mathcal{S}}_i, \tag{26}$$

where A_i are functions of the restitution coefficient

$$\left.\begin{aligned}A_1 &= \tfrac{6}{5}(1+\alpha)(3-\alpha)\\ A_2 &= \tfrac{1}{105}(1+\alpha)\{499-6\,\alpha[48+\alpha(5\,\alpha-11)]\}\\ A_3 &= \tfrac{1}{840}(1+\alpha)[5101-3597\,\alpha+1194\,\alpha^2-810\,\alpha^3]\end{aligned}\right\}. \tag{27}$$

Now we insert the deviation quantities $\tilde{\mathcal{Q}}_{ijk}$, $\tilde{\mathcal{R}}_{ij}$, and $\tilde{\mathcal{S}}_i$ as defined in Eq. (21) into the balance equations of $\mathcal{Q}_{ijk}$ [Eq. (22a)], $\mathcal{R}_{ij}$ [Eq. (22b)], and $\mathcal{S}_i$ [Eq. (22c)] and subsequently eliminate all the time derivatives of the 14-field variables (ρ, $\rho\,u_i$, θ, σ_{ij}, q_i, Δ) using their corresponding transport

equations, Eqs. (7a)–(7f). After some simple algebra and with the help of the source terms in Eq. (26), the following set of evolution equations is obtained for $\widetilde{\mathcal{Q}}_{ijk}$, $\widetilde{\mathcal{R}}_{ij}$, and $\widetilde{\mathcal{S}}_i$:

$$\mathcal{L}\widetilde{\mathcal{Q}}_{ijk} = -\varepsilon^{-1}\frac{A_1}{\tau_r}\,\widetilde{\mathcal{Q}}_{ijk}, \quad \mathcal{L}\widetilde{\mathcal{R}}_{ij} = -\varepsilon^{-1}\frac{A_2}{\tau_r}\,\widetilde{\mathcal{R}}_{ij}, \quad \mathcal{L}\widetilde{\mathcal{S}}_i = -\varepsilon^{-1}\frac{A_3}{\tau_r}\,\widetilde{\mathcal{S}}_i, \tag{28}$$

where the expressions of $\mathcal{L}\widetilde{\mathcal{Q}}_{ijk}$, $\mathcal{L}\widetilde{\mathcal{R}}_{ij}$, and $\mathcal{L}\widetilde{\mathcal{S}}_i$ are provided in Appendix C. Note that the term on the right-hand side of each equation in Eq. (28) has been multiplied by a factor "ε^{-1}"; this follows from the ansatz of scale separation: "the moments of the 14-moment system, i.e., σ_{ij}, q_i, and Δ, change on a timescale defined by τ_r, while all other higher-order moments $\mathcal{Q}_{ijk}$, $\mathcal{R}_{ij}$, and $\mathcal{S}_i$ change on a faster time scale $\varepsilon\,\tau_r$, where ε is a small parameter." Following this ansatz, Eqs. (28) are expanded in terms of the small parameter ε via

$$\left.\begin{aligned}\widetilde{\mathcal{Q}}_{ijk} &= \widetilde{\mathcal{Q}}^{(0)}_{ijk} + \varepsilon\,\widetilde{\mathcal{Q}}^{(1)}_{ijk} + \cdots\\ \widetilde{\mathcal{R}}_{ij} &= \widetilde{\mathcal{R}}^{(0)}_{ij} + \varepsilon\,\widetilde{\mathcal{R}}^{(1)}_{ij} + \cdots\\ \widetilde{\mathcal{S}}_{i} &= \widetilde{\mathcal{S}}^{(0)}_{i} + \varepsilon\,\widetilde{\mathcal{S}}^{(1)}_{i} + \cdots\end{aligned}\right\}, \tag{29}$$

which is a Chapman-Enskog-like expansion, with ε being the small parameter; for a detailed discussion, we refer to Ref. [35].

Inserting Eq. (29) into the balance laws Eq. (28) and comparing the terms of the same order in ε, it is straightforward to verify that the "leading-order" approximations of $\widetilde{\mathcal{Q}}_{ijk}$, $\widetilde{\mathcal{R}}_{ij}$, and $\widetilde{\mathcal{S}}_i$ resulting from balancing terms of order $O(\varepsilon^{-1})$, yields

$$\widetilde{\mathcal{Q}}^{(0)}_{ijk} = \widetilde{\mathcal{R}}^{(0)}_{ij} = \widetilde{\mathcal{S}}^{(0)}_{i} = 0, \tag{30}$$

which represent the original 14-moment system as discussed in Sec. II B. The first-order approximations of $\widetilde{\mathcal{Q}}_{ijk}$, $\widetilde{\mathcal{R}}_{ij}$, and $\widetilde{\mathcal{S}}_i$, resulting from balancing terms of order $O(\varepsilon^{0})$, can be written as

$$[\mathcal{L}\widetilde{\mathcal{Q}}_{ijk}]_{f_{14}} = -\frac{A_1}{\tau_r}\,\widetilde{\mathcal{Q}}^{(1)}_{ijk}, \quad [\mathcal{L}\widetilde{\mathcal{R}}_{ij}]_{f_{14}} = -\frac{A_2}{\tau_r}\,\widetilde{\mathcal{R}}^{(1)}_{ij}, \quad [\mathcal{L}\widetilde{\mathcal{S}}_{i}]_{f_{14}} = -\frac{A_3}{\tau_r}\,\widetilde{\mathcal{S}}^{(1)}_{i}, \tag{31}$$

where the notation $[\cdot]_{f_{14}}$ indicates that all moments inside the square brackets are evaluated with the 14-field distribution function f_{14} as given by Eq. (13). For example, the constitutive relations for higher-order terms in Eq. (24) [that appear on the left-hand side of Eq. (31)] and others are found as

$$\left.\begin{aligned}\mathcal{R}_{ijkl|14} = \mathcal{N}_{ijk|14} = 0, \quad \mathcal{M}^{(6)}_{ij|14} = 35\,\rho\,\theta^3\,(1+3\,\Delta)\,\delta_{ij} + 63\,\theta^2\,\sigma_{ij}\\ \widetilde{\mathcal{Q}}_{ijk|14} = \widetilde{\mathcal{R}}_{ij|14} = \widetilde{\mathcal{S}}_{i|14} = 0\end{aligned}\right\}. \tag{32}$$

Inserting Eq. (32) into Eq. (31) and rearranging different terms, we obtain the expressions for the deviation terms, after setting $\varepsilon = 1$, as

$$\widetilde{\mathcal{Q}}_{ijk} \equiv \widetilde{\mathcal{Q}}^{(1)}_{ijk} = -\frac{3\,\tau_r}{A_1}\left[\theta\,\frac{\partial\sigma_{\langle ij}}{\partial x_{k\rangle}} - \theta\,\sigma_{\langle ij}\,\frac{\partial\ln\rho}{\partial x_{k\rangle}} - \frac{\sigma_{\langle ij}}{\rho}\,\frac{\partial\sigma_{k\rangle l}}{\partial x_l} + \frac{4}{5}\,q_{\langle i}\,\frac{\partial u_{k\rangle}}{\partial x_j}\right], \tag{33a}$$

$$\begin{aligned}\widetilde{\mathcal{R}}_{ij} \equiv \widetilde{\mathcal{R}}^{(1)}_{ij} = -\frac{\tau_r}{A_2}\Bigg[&7\,\theta\,\sigma^s_{ij} - \frac{7}{\rho}\sigma_{ij}\,\mathcal{D} + \frac{28}{5}\,\theta\,\frac{\partial q_{\langle i}}{\partial x_{j\rangle}} + \frac{28}{5}\,q_{\langle i}\,\frac{\partial\theta}{\partial x_{j\rangle}} - \frac{28}{5}\,\theta\,q_{\langle i}\,\frac{\partial\ln\rho}{\partial x_{j\rangle}}\\ &- \frac{28}{5\,\rho}\,q_{\langle i}\,\frac{\partial\sigma_{j\rangle k}}{\partial x_k} + 4\,\theta\,\sigma_{k\langle i}\frac{\partial u_{j\rangle}}{\partial x_k} + 4\,\theta\,\sigma_{k\langle i}\,\frac{\partial u_k}{\partial x_{j\rangle}} - \frac{8}{3}\,\theta\,\sigma_{ij}\frac{\partial u_k}{\partial x_k}\\ &- \frac{14}{3\,\rho}\,\sigma_{ij}\,\sigma_{kl}\,\frac{\partial u_k}{\partial x_l} - \frac{14}{3\,\rho}\,\sigma_{ij}\,\frac{\partial q_k}{\partial x_k} + 14\,\rho\,\theta^2\,\Delta\,\frac{\partial u_{\langle i}}{\partial x_{j\rangle}}\Bigg],\end{aligned} \tag{33b}$$

$$\widetilde{\mathcal{S}}_i \equiv \widetilde{\mathcal{S}}_i^{(1)} = -\frac{\tau_r}{A_3}\Bigg[28\,\theta\,q_i^s - \frac{28}{\rho}\,q_i\,\mathcal{D} + 140\,\rho\,\theta^2\,\Delta\,\frac{\partial\theta}{\partial x_i} + 28\,\theta\,\sigma_{ij}\,\frac{\partial\theta}{\partial x_j} + 35\,\rho\,\theta^3\,\frac{\partial\Delta}{\partial x_i}$$
$$- 35\,\theta^2\,\Delta\,\frac{\partial\sigma_{ij}}{\partial x_j} - \frac{56}{3}\left(\frac{q_i}{\rho}\,\frac{\partial q_j}{\partial x_j} + \theta\,q_i\,\frac{\partial u_j}{\partial x_j} + \frac{q_i}{\rho}\,\sigma_{jk}\,\frac{\partial u_j}{\partial x_k}\right)$$
$$+ \frac{56}{5}\,\theta\left(q_i\,\frac{\partial u_j}{\partial x_j} + q_j\frac{\partial u_i}{\partial x_j} + q_j\,\frac{\partial u_j}{\partial x_i}\right)\Bigg]. \tag{33c}$$

2. *Regularized 14-moment (R14) equations*

The above corrections, Eqs. (33a)–(33c), must be substituted into the balance equations for the stress tensor, the heat-flux vector, and the contracted fourth-order moment, which read

$$\frac{\partial\sigma_{ij}}{\partial t} + \frac{\partial(\sigma_{ij}\,u_k)}{\partial x_k} + \frac{4}{5}\frac{\partial q_{\langle i}}{\partial x_{j\rangle}} + 2\,p\,\frac{\partial u_{\langle i}}{\partial x_{j\rangle}} + 2\,\sigma_{k\langle i}\frac{\partial u_{j\rangle}}{\partial x_k} + \underline{\frac{\partial\widetilde{\mathcal{Q}}_{ijk}}{\partial x_k}} = \sigma_{ij}^s, \tag{34a}$$

$$\frac{\partial q_i}{\partial t} + \frac{\partial(q_i\,u_j)}{\partial x_j} + \frac{5}{2}\,\sigma_{ij}\,\frac{\partial\theta}{\partial x_j} + \frac{5}{2}\,\rho\,\theta\,\frac{\partial\theta}{\partial x_i} + \theta\,\frac{\partial\sigma_{ij}}{\partial x_j} - \frac{\sigma_{ij}}{\rho}\,\frac{\partial\sigma_{jk}}{\partial x_k} - \sigma_{ij}\,\theta\,\frac{\partial\ln\rho}{\partial x_j}$$
$$+ \frac{5}{2}\,\frac{\partial(\rho\,\theta^2\,\Delta)}{\partial x_i} + \frac{7}{5}\,q_j\frac{\partial u_i}{\partial x_j} + \frac{2}{5}\,q_i\frac{\partial u_j}{\partial x_j} + \frac{2}{5}\,q_k\frac{\partial u_k}{\partial x_i} + \underline{\frac{1}{2}\frac{\partial\widetilde{\mathcal{R}}_{ij}}{\partial x_j} + \widetilde{\mathcal{Q}}_{ijk}\,\frac{\partial u_j}{\partial x_k}} = q_i^s, \tag{34b}$$

$$15\,\rho\,\theta^2\left(\frac{\partial\Delta}{\partial t} + u_i\,\frac{\partial\Delta}{\partial x_i}\right) + 4\,(2-5\,\Delta)\,\theta\left(\frac{\partial q_i}{\partial x_i} + \sigma_{ij}\frac{\partial u_i}{\partial x_j}\right) + 20\,q_i\,\frac{\partial\theta}{\partial x_i}$$
$$- \frac{8}{\rho}\,q_i\left(\frac{\partial\sigma_{ij}}{\partial x_j} + \theta\,\frac{\partial\rho}{\partial x_i}\right) + \underline{\frac{\partial\widetilde{\mathcal{S}}_i}{\partial x_i} + 4\,\widetilde{\mathcal{R}}_{ij}\,\frac{\partial u_i}{\partial x_j}} = \Delta^s. \tag{34c}$$

The underlined terms in Eqs. (34a)–(34c) are of higher order and are called "regularization" terms that are absent in the original 14-moment theory [see Eqs. (7a)–(7f)].

This completes the derivation of the full set of regularized equations for the 14-field variables (ρ, u_i, θ, σ_{ij}, q_i, Δ), which consist of Eqs. (7a)–(7c) and Eqs. (34a)–(34c) with higher-order terms given by Eqs. (33a)–(33c). From now onwards we refer to these equations as the R14 equations, where "R" stands for "regularized" and 14 denotes the number of field variables.

C. Regularized 13-moment (R13) equations

For the well-known 13-moment theory of Grad [28], the variables under consideration are ρ, $\rho\,u_i$, θ, σ_{ij}, and q_i. Hence the balance equations for 13-field variables of a dilute granular gas are the same as in Eqs. (7a)–(7e), and the stress and heat-flux equations are not closed due to the presence of higher-order moments $\mathcal{Q}_{ijk}$, $\mathcal{R}$, and $\mathcal{R}_{ij}$ for which we need to derive approximate expressions via the same regularization procedure as discussed in the previous section.

For the 13-moment theory, the distribution function

$$f|_{13} = f^M\left[1 + \frac{\sigma_{ij}}{2\rho\theta^2}C_iC_j + \frac{q_i}{5\rho\theta^3}(C^2 - 5\theta)C_i\right] \tag{35}$$

is used to evaluate the constitutive relations for the higher-order moments given by

$$\mathcal{Q}_{ijk|13} = 0, \quad \mathcal{R}_{|13} = 15\,\rho\,\theta^2, \quad \mathcal{R}_{ij|13} = 7\,\theta\,\sigma_{ij}, \tag{36}$$

and the expressions for linear source terms are

$$\left.\begin{aligned}\mathcal{D}_{|13} &= \tfrac{4}{3\,\tau_r}\,(1-\alpha^2)\,\rho\,\theta \equiv \mathcal{D}_{|14}(\Delta=0)\\ \sigma^s_{ij_{|13}} &= -\tfrac{4}{5\,\tau_r}\,(1+\alpha)\,(3-\alpha)\,\sigma_{ij} \equiv \sigma^s_{ij_{|14}}(\Delta=0)\\ q^s_{i_{|13}} &= -\tfrac{1}{15\,\tau_r}\,(1+\alpha)\,(49-33\,\alpha)\,q_i\end{aligned}\right\}. \tag{37}$$

Note that $\mathcal{D}_{|13}$, $\sigma^s_{ij_{|13}}$, and $q^s_{i_{|13}}$ all can also be obtained from Eqs. (15a)–(15c) by setting $\Delta = 0$. Therefore, the extended-hydrodynamic equations at the 13-moment level consist of Eqs. (7a)–(7e), supplemented with constitutive relations Eq. (36) and source terms Eq. (37).

To derive the "regularized" 13-moment system for a dilute granular gas, we introduce the deviations of $\mathcal{Q}_{ijk}$, $\mathcal{R}_{ij}$, and $\mathcal{R}$ from their values evaluated from the 13-moment nonequilibrium distribution function, Eq. (35), as

$$\left.\begin{aligned} \widetilde{\mathcal{Q}}_{ijk} &= \mathcal{Q}_{ijk} - \mathcal{Q}_{ijk|_{13}} = \mathcal{Q}_{ijk} \\ \widetilde{\mathcal{R}}_{ij} &= \mathcal{R}_{ij} - \mathcal{R}_{ij|_{13}} = \mathcal{R}_{ij} - 7\,\theta\,\sigma_{ij} \\ \widetilde{\mathcal{R}} &= \mathcal{R} - \mathcal{R}_{|_{13}} = \mathcal{R} - 15\,\rho\,\theta^2 \end{aligned}\right\}, \tag{38}$$

such that the above deviation quantities will vanish for the 13-moment approximation. Following the same procedure adopted in Sec. III B, we derived the nonzero approximations for the deviation quantities:

$$\widetilde{\mathcal{Q}}_{ijk} = \widetilde{\mathcal{Q}}_{ijk|_{14}}, \quad \widetilde{\mathcal{R}}_{ij} = \widetilde{\mathcal{R}}_{ij|_{14}}(\Delta = 0), \tag{39a}$$

$$\widetilde{\mathcal{R}} = -\frac{480\,\tau_r}{A_4}\left[\theta\,\frac{\partial q_i}{\partial x_i} + \frac{5}{2}\,q_i\,\frac{\partial\theta}{\partial x_i} + \theta\,\sigma_{ij}\,\frac{\partial u_i}{\partial x_j} - \theta\,q_i\,\frac{\partial \ln\rho}{\partial x_j} - \frac{q_i}{\rho}\,\frac{\partial\sigma_{ij}}{\partial x_j} - \frac{15}{4}\theta\,\mathcal{D}_{|13}\right] - \frac{240}{A_4}\,\rho\,\theta^2\,(2\,\alpha^2 + 9)\,(1-\alpha^2), \tag{39b}$$

where

$$A_4 = (1+\alpha)\,[30\,\alpha^2\,(1-\alpha) + 271 - 207\,\alpha]. \tag{40}$$

Note that $\widetilde{\mathcal{Q}}_{ijk}$ and $\widetilde{\mathcal{R}}_{ij}$ are the same as in R14 equations (33a)–(33b) with $\Delta = 0$. When the restitution coefficient is set to unity (i.e., $\alpha = 1$ for a molecular gas), the above terms are found to coincide with those derived by Struchtrup [31]. These correction terms are inserted into the transport equations for the stress tensor and heat flux vector [Eqs. (7d)–(7e)] to arrive at the regularized version of Grad's 13-moment theory (R13 equations) for a granular gas.

D. Regularized 10-moment (R10) equations

The variables under consideration in the 10-moment system [26,28,48] are the moments ρ, $\rho\,u_i$, θ, and σ_{ij}. Hence the balance equations for this system $(\rho, \rho\,u_i, \theta, \sigma_{ij})$ of dilute granular gas read as

$$\frac{\partial\rho}{\partial t} + \frac{\partial(\rho\,u_i)}{\partial x_i} = 0, \tag{41a}$$

$$\frac{\partial(\rho\,u_i)}{\partial t} + \frac{\partial\left(\rho\,u_i\,u_j\right)}{\partial x_j} + \frac{\partial p}{\partial x_i} + \frac{\partial\sigma_{ij}}{\partial x_j} = 0, \tag{41b}$$

$$\rho\left(\frac{\partial\theta}{\partial t} + u_i\,\frac{\partial\theta}{\partial x_i}\right) + \frac{2}{3}\left(\rho\,\theta\,\frac{\partial u_i}{\partial x_i} + \sigma_{ij}\frac{\partial u_i}{\partial x_j} + \underline{\frac{\partial q_i}{\partial x_i}}\right) = -\mathcal{D}_{|10}, \tag{41c}$$

$$\frac{\partial\sigma_{ij}}{\partial t} + \frac{\partial(\sigma_{ij}\,u_k)}{\partial x_k} + 2\,p\,\frac{\partial u_{\langle i}}{\partial x_{j\rangle}} + 2\,\sigma_{k\langle i}\frac{\partial u_{j\rangle}}{\partial x_k} + \underline{\frac{4}{5}\frac{\partial q_{\langle i}}{\partial x_{j\rangle}} + \frac{\partial\mathcal{Q}_{ijk}}{\partial x_k}} = \sigma^s_{ij_{|10}}, \tag{41d}$$

where the underlined terms q_i (heat flux) and $\mathcal{Q}_{ijk}$ (deviatoric third moment) are of higher order which vanish identically,

$$q_{i|10} = 0, \quad \mathcal{Q}_{ijk|10} = 0, \tag{42}$$

for the 10-moment distribution function [28]

$$f|_{10} = f^M\left(1 + \frac{\sigma_{ij}}{2\rho\theta^2}C_iC_j\right). \tag{43}$$

With the help of Eq. (43), the collisional source terms in Eqs. (41c)–(41d) are evaluated,

$$\mathcal{D}_{|10} \equiv \mathcal{D}_{|13} \quad \text{and} \quad \sigma^s_{ij_{|10}} \equiv \sigma^s_{ij_{|13}}, \tag{44}$$

as in Eq. (37). Therefore, the 10-moment system consists of Eqs. (41a)–(41d) in the absence of underlined terms; i.e., the heat flux is identically zero for the 10-moment system.

Regularized 10-moment equations can be derived by using the same procedure discussed in Sec. III B. The corrections to 10-moment equations are obtained as

$$q_i = -\frac{\tau_r}{A_5}\left[\frac{5}{2}\rho\,\theta\,\frac{\partial\theta}{\partial x_i} + \frac{5}{2}\,\sigma_{ij}\,\frac{\partial\theta}{\partial x_j} + \theta\,\frac{\partial\sigma_{ij}}{\partial x_j} - \theta\,\sigma_{ij}\,\frac{\partial\ln\rho}{\partial x_j} - \frac{\sigma_{ij}}{\rho}\,\frac{\partial\sigma_{jk}}{\partial x_k}\right], \tag{45a}$$

$$\mathcal{Q}_{ijk} = -\frac{3\,\tau_r}{A_1}\left[\theta\,\frac{\partial\sigma_{\langle ij}}{\partial x_{k\rangle}} - \theta\,\sigma_{\langle ij}\,\frac{\partial\ln\rho}{\partial x_{k\rangle}} - \frac{\sigma_{\langle ij}}{\rho}\,\frac{\partial\sigma_{k\rangle l}}{\partial x_l}\right], \tag{45b}$$

where

$$A_5 = \tfrac{1}{15}(1+\alpha)(49 - 33\alpha). \tag{46}$$

The above expressions for the heat flux (q_i) and the deviatoric third moment (Q_{ijk}) must be inserted into the energy equation (41c) and the stress tensor equation (41d) to obtain the complete set of "regularized" equations for the 10 fields ($\rho, u_i, \theta, \sigma_{ij}$) that consist of Eqs. (41a)–(41d), with higher-order terms given by Eqs. (45a) and (45b). We refer to these equations as the R10 (regularized 10-moment) equations. It should be noted that the recent work of one of the present authors [26,49–52] demonstrated the superiority of the 10-moment theory (based on anisotropic Maxwellian distribution function that follows from the maximum entropy principle) in accurately predicting the rheology of homogeneously sheared granular suspensions. The remaining part of this paper deals with validating the present R10 equations for the plane shock-wave problem [53] in both molecular and granular gases.

IV. PLANE SHOCK WAVES AND THE RANKINE-HUGONIOT CONDITIONS: R10 EQUATIONS

To illustrate the advantage of regularized equations, we consider the regularized version of 10-moment (R10) equations and formulate the Riemann problem of planar shock waves propagating through molecular and granular gases. To solve this problem, the resulting equations must be supplemented by Rankine-Hugoniot conditions [43] as discussed in Sec. IV B.

A. One-dimensional form of R10 equations

For the plane shock-wave problem, the one-dimensional balance equations for the R10-moment system involve four field variables, namely, the density $\rho(x,t)$, the velocity $u(x,t)$, the temperature $\theta(x,t)$, and the longitudinal stress $\sigma(x,t) \equiv \sigma_{xx}(x,t)$. The one-dimensional equations for the R10-moment model are

$$\frac{\partial\rho}{\partial t} + \frac{\partial}{\partial x}(\rho\,u) = 0, \tag{47a}$$

$$\frac{\partial}{\partial t}(\rho\,u) + \frac{\partial}{\partial x}(\rho\,u^2 + \rho\,\theta + \sigma) = 0, \tag{47b}$$

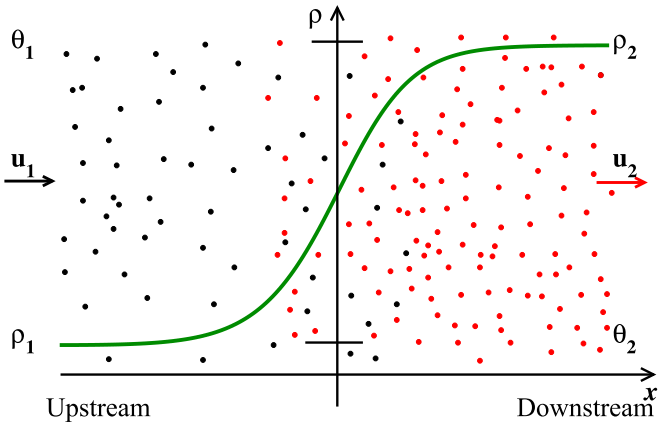

FIG. 3. Schematic of the Riemann problem of a plane shock wave: the upstream and downstream properties of the shock are denoted by (ρ_1, u_1, θ_1) and (ρ_2, u_2, θ_2), respectively. The green line represents a typical density profile across the shock.

$$\frac{\partial}{\partial t}(\rho\, u^2 + 3\,\rho\,\theta) + \frac{\partial}{\partial x}(\rho\, u^3 + 5\,\rho\,\theta\, u + 2\,\sigma\, u + \underline{2\, q}) = -3\,\mathcal{D}, \tag{47c}$$

$$\frac{\partial}{\partial t}\left(\frac{2}{3}\,\rho\, u^2 + \sigma\right) + \frac{\partial}{\partial x}\left(\frac{2}{3}\,\rho\, u^3 + \frac{4}{3}\,\rho\,\theta\, u + \frac{7}{3}\,\sigma\, u + \underline{\frac{8}{15}\, q + \mathcal{Q}}\right) = \sigma^s, \tag{47d}$$

where the underlined nonzero terms (q and $\mathcal{Q}$) in Eq. (47c) and Eq. (47d) arise from the regularization procedure. The expressions for q (heat flux) and $\mathcal{Q}$ (deviatoric third moment) and the source terms $\mathcal{D}$ and σ^s are given by

$$q(x,t) \equiv q_x(x,t) = -\frac{\tau_r}{A_5}\left[\frac{5}{2}\,(\rho\,\theta + \sigma)\,\frac{\partial \theta}{\partial x} + \left(\theta - \frac{\sigma}{\rho}\right)\frac{\partial \sigma}{\partial x} - \theta\,\sigma\,\frac{\partial \ln \rho}{\partial x}\right], \tag{48a}$$

$$\mathcal{Q}(x,t) \equiv \mathcal{Q}_{xxx}(x,t) = -\frac{9\,\tau_r}{5\,A_1}\left[\left(\theta - \frac{\sigma}{\rho}\right)\frac{\partial \sigma}{\partial x} - \theta\,\sigma\,\frac{\partial \ln \rho}{\partial x}\right], \tag{48b}$$

$$\mathcal{D}(x,t) = \frac{4}{3}\frac{d^2}{m}\sqrt{\pi}\,(1-\alpha^2)\,\rho^2\,\theta^{\frac{3}{2}}, \tag{48c}$$

$$\sigma^s(x,t) = -\frac{4}{5}\frac{d^2}{m}\sqrt{\pi\,\theta}\,(1+\alpha)\,(3-\alpha)\,\rho\,\sigma. \tag{48d}$$

B. Rankine-Hugoniot relations for molecular and granular gases

Let us denote the upstream ($x \to -\infty$) very far ahead of a shock and the downstream ($x \to \infty$) very far behind a shock, located at $x = 0$, by (ρ_1, u_1, θ_1) and (ρ_2, u_2, θ_2), respectively; see the sketch in Fig. 3. The finite jump in each state variable across a shock is given by the so-called Rankine-Hugoniot (RH) relations [43], which can be obtained from the balance equations of mass, momentum, and energy by applying the standard method [43] and using the fact that the terms which are independent of gradients of the hydrodynamic variables do not contribute to RH conditions [11,21,43]. In the stationary coordinate frame of the shock (i.e., the reference coordinate frame is moving with the shock speed), these equations are [48]

$$\rho_1\, u_1 = \rho_2\, u_2, \tag{49a}$$

$$\rho_1\, u_1^2 + \rho_1\,\theta_1 + \sigma_1 = \rho_2\, u_2^2 + \rho_2\,\theta_2 + \sigma_2, \tag{49b}$$

$$\rho_1\, u_1^3 + 5\,\rho_1\,\theta_1\, u_1 + 2\,\sigma_1\, u_1 + 2\, q_1 = \rho_2\, u_2^3 + 5\,\rho_2\,\theta_2\, u_2 + 2\,\sigma_2\, u_2 + 2\, q_2. \tag{49c}$$

These relations provide necessary conditions for any solution of the system (47a)–(47d). The conditions given in Eqs. (49a)–(49c) can be further simplified by assuming that the end states are in "local" equilibrium such that the higher-order moment variables σ and q vanish at upstream and downstream end states for a molecular gas. One thing we need to point out here is that there is no equilibrium state in granular gas, which in contrast to the molecular gas. So an additional ansatz [11] is now made: the upstream and downstream states are *spatially uniform*, along with a temporally decaying temperature field, which represents the "local" equilibrium of a granular gas [3], known as the *homogeneous cooling state*. The spatial homogeneity of end states implies that the flux terms σ and q vanish at $x \to \pm\infty$. Therefore, substituting these boundary conditions in Eqs. (49a)–(49c) we arrive at the RH conditions for a granular/molecular gas,

$$\rho_1 u_1 = \rho_2 u_2, \tag{50a}$$

$$\rho_1 u_1^2 + \rho_1 \theta_1 = \rho_2 u_2^2 + \rho_2 \theta_2, \tag{50b}$$

$$\rho_1 u_1^3 + 5\rho_1 \theta_1 u_1 = \rho_2 u_2^3 + 5\rho_2 \theta_2 u_2. \tag{50c}$$

The local Mach number Ma is defined as the ratio of velocity of the gas to the speed of sound through the molecular gas/granular gas [21]

$$\mathrm{Ma} = \frac{|u|}{c} \equiv \frac{|u|}{\sqrt{\gamma\,\theta}}, \tag{51}$$

where γ is the adiabatic index, which is the ratio between two specific heats, and $c = \sqrt{\gamma\theta}$ is the adiabatic sound speed, which is also the characteristic slope [43] obtained from Euler equations. The numerical value of the adiabatic index γ for a monatomic granular gas is 5/3, which is the same as that for a molecular gas [21].

Unlike for molecular gases we have to specify the RH conditions (boundary conditions) for a granular gas at time $t = 0$ [11,48,54]. The initial ($t = 0$) shock profiles are given by (ρ_1, u_1, θ_1) for $x \leqslant 0$ and (ρ_2, u_2, θ_2) for $x > 0$, and the shock speed is zero at $t = 0$. Assuming that the flow is adiabatic and solving the RH relations (50a), the downstream quantities can be expressed as in terms of their upstream counterparts. The ratio of downstream to upstream density, velocity, and granular temperature are given as [48]

$$\frac{\rho_2(t=0)}{\rho_1(t=0)} = \frac{(\gamma+1)\mathrm{Ma}_1^2}{2+(\gamma-1)\mathrm{Ma}_1^2}, \tag{52a}$$

$$\frac{u_2(t=0)}{u_1(t=0)} = \frac{2+(\gamma-1)\mathrm{Ma}_1^2}{(\gamma+1)\mathrm{Ma}_1^2}, \tag{52b}$$

$$\frac{\theta_2(t=0)}{\theta_1(t=0)} = \frac{\left[2\gamma\mathrm{Ma}_1^2-(\gamma-1)\right]\left[(\gamma-1)\mathrm{Ma}_1^2+2\right]}{(\gamma+1)^2\mathrm{Ma}_1^2}, \tag{52c}$$

where $\mathrm{Ma}_1 = u_1(0)/\sqrt{\gamma\,\theta_1(0)}$ is the upstream Mach number at $t = 0$. For the Riemann problem, the local Mach number is maximum at the upstream state and decreases through the shock by reaching its minimum value at the downstream state.

V. SHOCK PROFILES FROM R10 EQUATIONS IN A MOLECULAR GAS

A. Numerical results of R10 model

Here we present results for the Riemann problem of planar shock waves in a molecular gas by solving the R10-moment equations, and the results are compared with those obtained from the standard 10-moment equations. The equations are made dimensionless by the upstream state variables (see Fig. 3) as detailed in Appendix D. The upstream boundary conditions for this plane

shock-wave problem are taken as

$$\rho_1 = 1, \quad u_1 = \mathrm{Ma}_1\sqrt{\gamma}, \quad \theta_1 = 1, \quad \sigma_1 = 0, \tag{53}$$

while the downstream boundary conditions are provided by RH jump conditions, which are given by

$$\rho_2 = \frac{(\gamma+1)\mathrm{Ma}_1^2}{2+(\gamma-1)\mathrm{Ma}_1^2}\,\rho_1, \tag{54a}$$

$$u_2 = \frac{2+(\gamma-1)\mathrm{Ma}_1^2}{(\gamma+1)\mathrm{Ma}_1^2}\,u_1, \tag{54b}$$

$$\theta_2 = \frac{\left[2\gamma\mathrm{Ma}_1^2-(\gamma-1)\right]\left[(\gamma-1)\mathrm{Ma}_1^2+2\right]}{(\gamma+1)^2\mathrm{Ma}_1^2}\,\theta_1, \tag{54c}$$

$$\sigma_2 = 0. \tag{54d}$$

First, we perform numerical simulations of shock waves in a molecular gas using the numerical scheme of Refs. [55,56], the details of which are given in Appendix D and can also be found in Ref. [48]. We have carried out simulations by considering a one-dimensional domain of length $L = 50$ covering $x \in (-25, 25)$ with 2000 grid points and placing the initial discontinuity at $x = 0$; the time step is taken to be $\Delta t = \mathcal{C}\Delta x/max(a_i)$, where $\mathcal{C}$ is the Courant-Friedrichs-Lewy (CFL) number, Δx is the grid size, and a_i are the eigenvalues of the relaxation matrix (see Appendix D). It must be pointed out that the CFL number should be very small for both Navier-Stokes and 10-moment models. For present computations of shocks in molecular gases, we take the CFL number as 0.01, which gives converged solutions.

1. Validation of the numerical scheme

In order to validate the shock profiles obtained from the present numerical scheme for PDEs as discussed in Appendix D, we have also calculated the normalized density from the following ODE:

$$\frac{d\rho}{dx} = -\frac{\rho^3\sigma^s}{3C_1C_2\left(\rho-\frac{4C_1^2}{3C_2}\right)}, \tag{55}$$

where

$$C_1 = \rho u = \rho_1 u_1 \quad \text{and} \quad C_2 = \rho u^2 + \rho\theta + \sigma = \left(\gamma\mathrm{Ma}_1^2+1\right)\rho_1\theta_1. \tag{56}$$

Equation (55) has been derived from the 10-moment model for the stationary shock-wave problem; see Appendix A for details. This constitutes an initial-value problem which is solved numerically by using the standard fourth-order Runge-Kutta method. As discussed in Appendix A, at the critical Mach number, $\mathrm{Ma}_1 = 3/\sqrt{5}$, the solution to Eq. (55) attains an infinite slope. Care must be taken while solving Eq. (55) since a discontinuity needs to be embedded in the (weak) solution at $\mathrm{Ma}_1 > \mathrm{Ma}_{\mathrm{cr}}$. If the upstream Mach number is above the critical Mach number, then the initial value for ρ becomes its frozen jump value ρ_J and is given by [48,57]

$$\rho_J = \frac{2\gamma\,\mathrm{Ma}_1^2}{\gamma\,\mathrm{Ma}_1^2+3}. \tag{57}$$

This implies that when $\mathrm{Ma}_1 > 3/\sqrt{5}$, the upstream state is connected by a jump to the shock state ρ_J, which is then connected to the downstream state.

Figure 4 displays a comparison between (1) the numerical solution of Eq. (55), called the "ODE solution" (black circled lines), and (2) the corresponding "PDE solution" (red-circled lines),

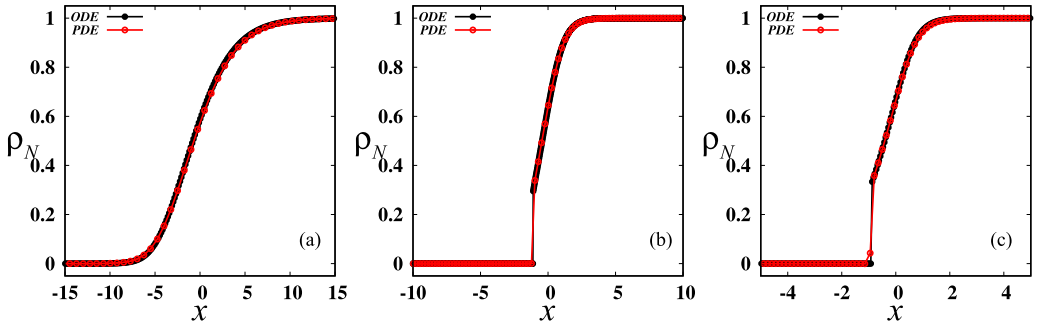

FIG. 4. Normalized density profiles ρ_N [Eq. (58)] in a molecular gas predicted by 10-moment model using two different numerical methods; see the text for details: (a) $\mathrm{Ma}_1 = 1.2$, (b) $\mathrm{Ma}_1 = 2$, and (c) $\mathrm{Ma}_1 = 3$.

obtained by numerically solving Eq. (47) using the relaxation scheme (see Appendix D). The density has been normalized using the following relation:

$$\rho_N = \frac{\rho - \rho_1}{\rho_2 - \rho_1}. \tag{58}$$

The left, middle, and rights panels of Fig. 4 correspond to Mach numbers of 1.2, 2, and 3, respectively; for all cases, we set $\alpha = 1$, which refers to a molecular gas. While the density profile remains smooth across the shock at $\mathrm{Ma}_1 = 1.2$, the discontinuous shock profiles are expectedly found at $\mathrm{Ma}_1 = 2$ and 3 since both cases belong to $\mathrm{Ma}_1 > \mathrm{Ma}_{\mathrm{cr}} \approx 1.34$. For all cases, there is an excellent agreement between the ODE solution and the PDE solution, including the jump discontinuity. Collectively, Fig. 4 validates the relaxation-type numerical scheme presented in Appendix D that we have used to solve the PDE system for the one-dimensional shock-wave problem (the latter is required for the granular shock problem as we shall see in Sec. VI). It also confirms that the relaxation-type schemes are able to capture both smooth and discontinuous shock solutions of extended hydrodynamic models.

2. Shock profiles from R10 model

Here we present numerical results on shock profiles for the regularized 10-moment model and compare them with those for the standard 10-moment model. Figure 5 shows the density, temperature, velocity, longitudinal stress ($\sigma = \sigma_{xx}$), heat flux [$q = q_x$, Eq. (48a)], and deviatoric third moment [$\mathcal{Q}$, Eq. (48b)] profiles as predicted by 10-moment and R10-moment models for an upstream Mach number $\mathrm{Ma}_1 = 2 > \mathrm{Ma}_{\mathrm{cr}}$; the DSMC data of Timokhin *et al.* [58] for density and temperature are also superimposed in Figs. 5(a) and 5(b). Note that the temperature and velocity profiles have been normalized via the following relations:

$$\theta_N = \frac{\theta - \theta_1}{\theta_2 - \theta_1}, \quad u_N = \frac{u - u_2}{u_1 - u_2}, \tag{59}$$

respectively, and the density by Eq. (58). It is seen in Fig. 5 that all profiles predicted by 10-moment model are steepened into a discontinuity on the upstream part of the shock, but this unwanted feature is not seen in the case of R10-moment profiles. Overall, the R10-moment model predicts the smooth/continuous shock profiles unlike the 10-moment model. Comparing the profiles predicted by the R10-moment model for both upstream Mach numbers $\mathrm{Ma}_1 = 1.2$ (not shown) and $\mathrm{Ma}_1 = 2$, we find that the profiles are less diffusive at the downstream end than at the upstream end. At $\mathrm{Ma}_1 > \mathrm{Ma}_{\mathrm{cr}}$, the 10-moment model produces discontinuous shock structure, whereas the

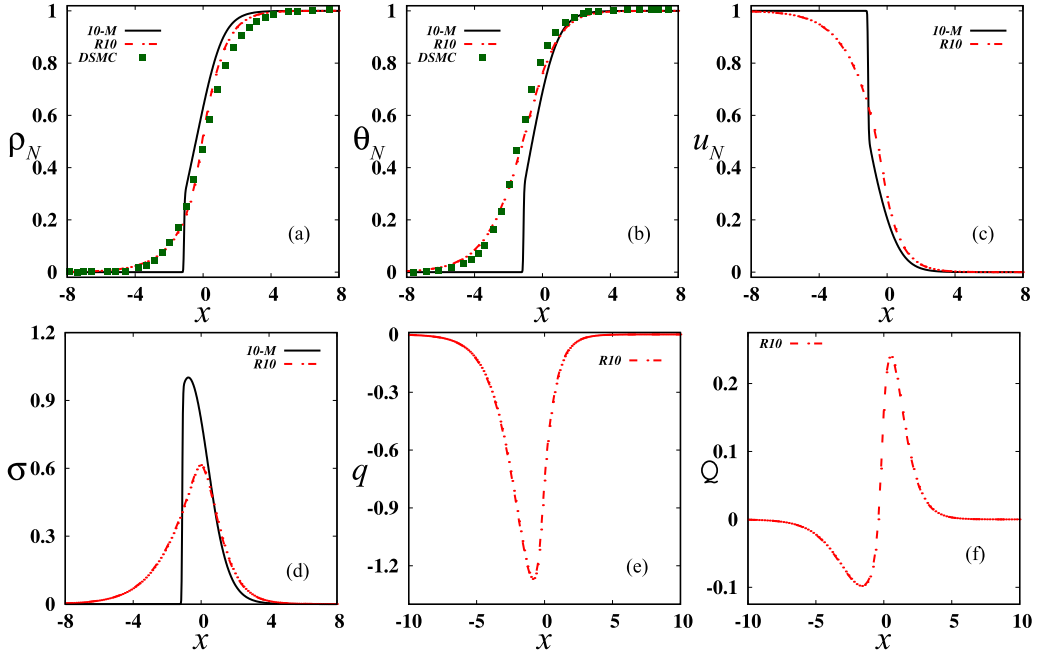

FIG. 5. Comparison of shock profiles for a molecular gas predicted by R10 (dot-dashed line) and 10-moment (solid line) model: (a) normalized density ρ_N [Eq. (58)], (b) temperature θ_N [Eq. (59)], (c) velocity u_N [Eq. (59)], (d) longitudinal stress $\sigma \equiv \sigma_{xx}$, (e) heat flux $q \equiv q_x$, and (f) deviatoric third moment $\mathcal{Q} \equiv \mathcal{Q}_{xxx}$ for an upstream Mach number of $\mathrm{Ma}_1 = 2 > \mathrm{Ma}_{\mathrm{cr}}$. The DSMC data of Timokhin *et al.* [58] for density and temperature are superimposed in panels (a) and (b).

R10-moment model produces a continuous shock structure, and the reason for the latter is explained below.

B. Origin of smooth shock solution in R10 equations

Here we reanalyze the R10 equations for a planar shock, Eqs. (47a)–(47d), moving at a constant speed; i.e., the shock is stationary in a reference frame which is moving with the shock speed, and hence the time derivatives vanish. For a planar stationary shock, the R10-moment equations (47) for a dilute granular gas boil down to the following:

$$\frac{d}{dx}(\rho u) = 0, \tag{60a}$$

$$\frac{d}{dx}(\rho u^2 + \rho\theta + \sigma) = 0, \tag{60b}$$

$$\frac{d}{dx}(\rho u^3 + 5\rho\theta u + 2\sigma u) = -3\,\mathcal{D} - 2\,\frac{dq}{dx}, \tag{60c}$$

$$\frac{d}{dx}\left(\frac{2}{3}\rho u^3 + \frac{4}{3}\rho\theta u + \frac{7}{3}\sigma u\right) = \sigma^s - \frac{8}{15}\,\frac{dq}{dx} - \frac{d\mathcal{Q}}{dx}. \tag{60d}$$

The boundary conditions for the above system of ODEs are supplied by the RH relations and $\sigma_1 = 0 = \sigma_2$ at both upstream and downstream ends.

Solving Eqs. (60a) and (60b), along with boundary conditions, we obtain $C_1 = \rho u = \rho_1 u_1$ and $C_2 = \rho u^2 + \rho\theta + \sigma = (\gamma \mathrm{Ma}_1^2 + 1)\rho_1\theta_1$. Using C_1 and C_2, Eqs. (60c)–(60d) can be combined to

obtain the following set of coupled ODEs for $\rho(x)$ and $\theta(x)$,

$$\frac{d\rho}{dx} = \frac{\rho^3}{3\left(\gamma \mathrm{Ma}_1^2 + 1\right) C_1\, \rho_1\, \theta_1} \left[\frac{\mathcal{D} - \sigma^s + \frac{6}{5}\frac{dq}{dx} + \frac{d\mathcal{Q}}{dx}}{\rho - \rho_c} \right], \tag{61a}$$

$$\frac{d\theta}{dx} = \frac{1}{3\, C_1} \left(-2\,\mathcal{D} - \sigma^s - \frac{4}{5}\frac{dq}{dx} + \frac{d\mathcal{Q}}{dx} \right) + \left(\frac{2\, C_1^2 - \rho\, C_2}{3\, \rho^3} \right) \frac{d\rho}{dx}, \tag{61b}$$

along with two algebraic equations,

$$u = \frac{C_1}{\rho}, \quad \sigma = C_2 - \frac{C_1^2}{\rho} - \rho\,\theta, \tag{62}$$

with the expression for the critical density ρ_c being given by Eq. (A6). The expressions for q, $\mathcal{Q}$, $\mathcal{D}$, and σ^s are given in Eqs. (48a)–(48d), respectively.

The spatial derivative of the "longitudinal" heat flux can be written as

$$\frac{dq}{dx} = -\frac{\tau_r}{A_5} \left[\frac{5}{2} (\rho\,\theta + \sigma) \frac{d^2\theta}{dx^2} + \left(\theta - \frac{\sigma}{\rho} \right) \frac{d^2\sigma}{dx^2} - \frac{\theta\sigma}{\rho} \frac{d^2\rho}{dx^2} \right] + \text{L.O.D.}, \tag{63}$$

where L.O.D. refers to terms of an lower-order derivative and their combinations. The second derivative of the longitudinal stress is expressed as

$$\frac{d^2\sigma}{dx^2} = \left(\frac{C_1^2}{\rho^2} - \theta \right) \frac{d^2\rho}{dx^2} - \rho \frac{d^2\theta}{dx^2} - 2 \left(\frac{C_1^2}{\rho^3} \frac{d\rho}{dx} + \frac{d\theta}{dx} \right) \frac{d\rho}{dx}. \tag{64}$$

Substituting this into Eq. (63), we obtain the leading-order expression

$$\frac{dq}{dx} = -\frac{\tau_r}{A_5} \left(\left[\frac{7}{2} \left(C_2 - \frac{C_1^2}{\rho} \right) - 2\rho\theta \right] \frac{d^2\theta}{dx^2} - \left\{ \frac{C_1^2}{\rho^3} \left[\left(C_2 - \frac{C_1^2}{\rho} \right) - 2\rho\theta \right] + \theta^2 \right\} \frac{d^2\rho}{dx^2} \right) + \text{L.O.D.}, \tag{65}$$

which contains second-order derivatives of density and temperature at the leading order. Similarly, the spatial derivative of the deviatoric third moment $d\mathcal{Q}/dx$ can be written as

$$\frac{d\mathcal{Q}}{dx} = -\frac{9\tau_r}{5A_1} \left(\left[\left(C_2 - \frac{C_1^2}{\rho} \right) - 2\rho\theta \right] \frac{d^2\theta}{dx^2} - \left\{ \frac{C_1^2}{\rho^3} \left[\left(C_2 - \frac{C_1^2}{\rho} \right) - 2\rho\theta \right] + \theta^2 \right\} \frac{d^2\rho}{dx^2} \right) + \text{L.O.D.} \tag{66}$$

The above analysis indicates that the presence of regularized terms like dq/dx and $d\mathcal{Q}/dx$ in Eqs. (60c)–(60d) results in second-order gradient terms $[\mathrm{d}^2\rho/dx^2, \mathrm{d}^2\theta/dx^2]$ in Eq. (61a), which smoothes the discontinuous density field, much like the addition of the diffusive term to the inviscid Burgers equation. Essentially these higher-order terms provide a length scale over which the original discontinuity is smoothed out.

VI. SHOCK PROFILES IN A GRANULAR GAS AND REREGULARIZATION OF R10 MODEL

To study shock-wave structures in a dilute granular gas, we consider a domain of length $L = 100$ covering $(-50, 50)$, filled with a granular gas of two different homogeneous cooling states at the left and right, namely, the upstream and downstream ends, respectively; the shock is positioned at $x = 0$ at $t = 0$. The upstream boundary conditions for a dilute granular gas are given in Eq. (53), and the downstream boundary conditions are provided by RH relations, Eq. (52). As discussed in Appendix D, the numerical computations are performed by using 10 000 grid points, with a CFL number of $\mathcal{C} = 0.001$ for all results presented below. For granular shocks ($\alpha < 1$), the upstream quantities at $t = 0$ are used as reference quantities [e.g. $\rho_R = \rho_1(0)$, $\theta_R = \theta_1(0)$, $u_R = \sqrt{\theta_1(0)}$, $L_R = l_1$ and $t_R = l_1/u_R$] to nondimensionalize all variables; see Appendix D for details.

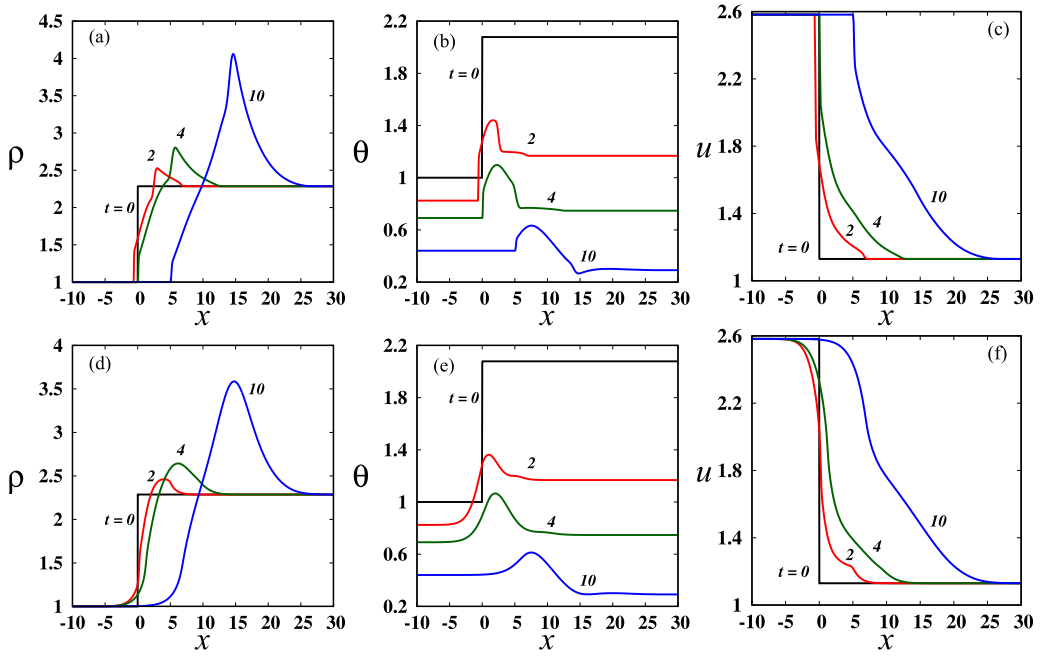

FIG. 6. Early-time evolutions of granular shock-wave profiles as predicted by 10-moment (upper panels) and R10 model (lower panels) for an upstream Mach number $\mathrm{Ma}_1 = 2$ and for a restitution coefficient of $\alpha = 0.9$: (a), (d) density, (b), (e) temperature, and (c), (f) velocity.

A. Early-time behavior of granular shock

We present the results on granular shock waves for two values of the upstream Mach number $\mathrm{Ma}_1 = 1.2$ and $\mathrm{Ma}_1 = 2$, and two values of the restitution coefficient $\alpha = 0.9$ and $\alpha = 0.7$. Early-time evolutions of granular density, temperature, and velocity profiles predicted by 10-moment [top row panels: (a), (b), and (c)] and R10 models [bottom row panels: (d), (e), and (f)] are displayed in Fig. 6 for an upstream Mach number of $\mathrm{Ma}_1 = 2$ and a restitution coefficient of $\alpha = 0.9$. Comparing Fig. 6(a) and Fig. 6(d), we make the following observations: (1) the density profiles predicted by the R10-moment model are smoother and more diffusive on the upstream side than the 10-moment model and (2) both 10-moment and R10-moment models predict a finite density overshoot,

$$\triangle\rho = \rho_{\max} - \rho_2 > 0, \tag{67}$$

within the shock layer, which is a novel feature of shock waves in a granular gas [11]; and (3) the R10 model predicts a lesser magnitude of the density overshoot ($\triangle\rho$) compared to the 10-moment model, and the density maximum ($\rho_{\max}$) increases with increasing upstream Mach number ($\mathrm{Ma}_1 \uparrow$) and decreasing restitution coefficient ($\alpha < 1$) for both models.

Figures 6(b) and 6(e) display the granular temperature profiles predicted by the 10-moment and R10-moment models for an upstream Mach number of $\mathrm{Ma}_1 = 2$ with a restitution coefficient of $\alpha = 0.9$. By comparing Figs. 6(b) and 6(e), we find that while the granular temperature profiles predicted by the R10 model are smoother, a steepened discontinuity at the upstream side of the shock can be seen in temperature profiles predicted by the 10-moment model; both models predict the temperature maximum $\theta_{\max}$ within the shock layer and a temperature minimum $\theta_{\min}$ (at $t = 10$) near the downstream edge of the shock layer. Note further that the R10 model predicts a lesser value of $\theta_{\max}$, compared to its prediction by the 10-moment model. The related temporal evolutions of the velocity profiles within the shock layer can be ascertained from Figs. 6(c) and 6(f).

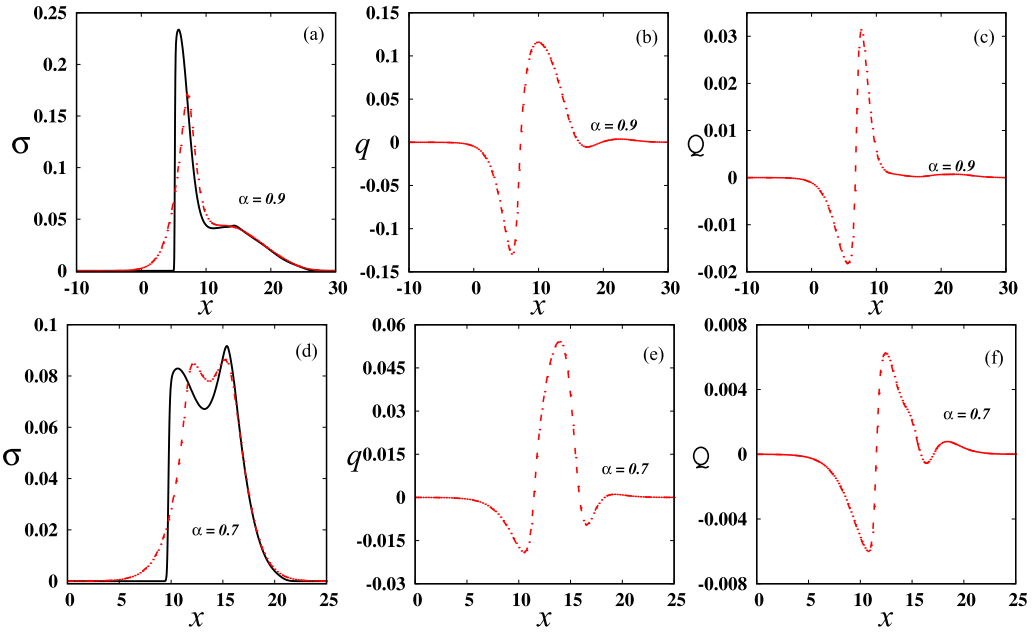

FIG. 7. Profiles of (a) longitudinal stress ($\sigma \equiv \sigma_{xx}$), (b) heat flux ($q \equiv q_x$), and (c) deviator of third-moment ($\mathcal{Q} \equiv \mathcal{Q}_{xxx}$) predicted by R10 (red dashed curve) and 10-moment (black curve) models for an upstream Mach number $\mathrm{Ma}_1 = 2$ and at time $t = 10$ for restitution coefficients of $\alpha = 0.9$ (upper panels) and $\alpha = 0.7$ (lower panels).

Figure 7 shows the predictions of 10-moment (black curves) and R10-moment (red curves) models for [Figs. 7(a) and 7(d)] the longitudinal stress σ, [Figs. 7(b) and 7(e)] the heat flux q, and [Figs. 7(c) and 7(f)] the third-moment deviator $\mathcal{Q}$ at a time $t = 10$ for $\mathrm{Ma}_1 = 2$; the upper panels (a–c) and lower panels (d–f) represent results for restitution coefficients of $\alpha = 0.9$ and $\alpha = 0.7$, respectively. Comparing Figs. 7(a) and 7(d), we find that the longitudinal stress profiles of the R10-moment model are smoother like the density and temperature profiles in Figs. 6(d) and 6(e). It is observed from all panels in Fig. 7 that the magnitudes of σ, q, and $\mathcal{Q}$ decrease with increasing dissipation (at a specified time), which can be tied to the faster relaxation with decreasing restitution coefficient α.

From the above comparisons for granular shock waves, we conclude that the regularized 10-moment model predicts smooth shock profiles beyond $\mathrm{Ma}_{cr|_{10}}$, unlike the standard 10-moment model. Both models predict a density overshoot ($\Delta\rho = \rho_{\max} - \rho_2 > 0$) and a temperature maximum ($\theta_{\max}$) within the shock layer; in particular, the R10 model predicts smaller values of the above quantities at a given time for specified values of Ma_1 and α.

B. Long-time behavior of granular shock: Need for second regularization?

The time evolution of the density overshoot $\Delta\rho$, Eq. (67), for $\mathrm{Ma}_1 = 1.2$ and $\alpha = 0.9$ is shown in Fig. 8(a); the black-dashed and red-dashed dot lines denote predictions of 10-moment and R10 models, respectively. We find that $\triangle\rho > 0$ in a granular gas and its magnitude increases with time; note that $(\triangle\rho)_{R10} < (\triangle\rho)_{10}$, except at very early times. We also verified (not shown) that $\triangle\rho$ increases as the upstream Mach number and/or the dissipation are increased. The inset of Fig. 8(a) indicates that the spatial location of $\rho_{\max}$ shifts to the right with time, from which a shock speed can be estimated. The speed of propagation of the density maximum is defined as

$$v_s = \frac{x(\rho = \rho_{\max})}{t}. \tag{68}$$

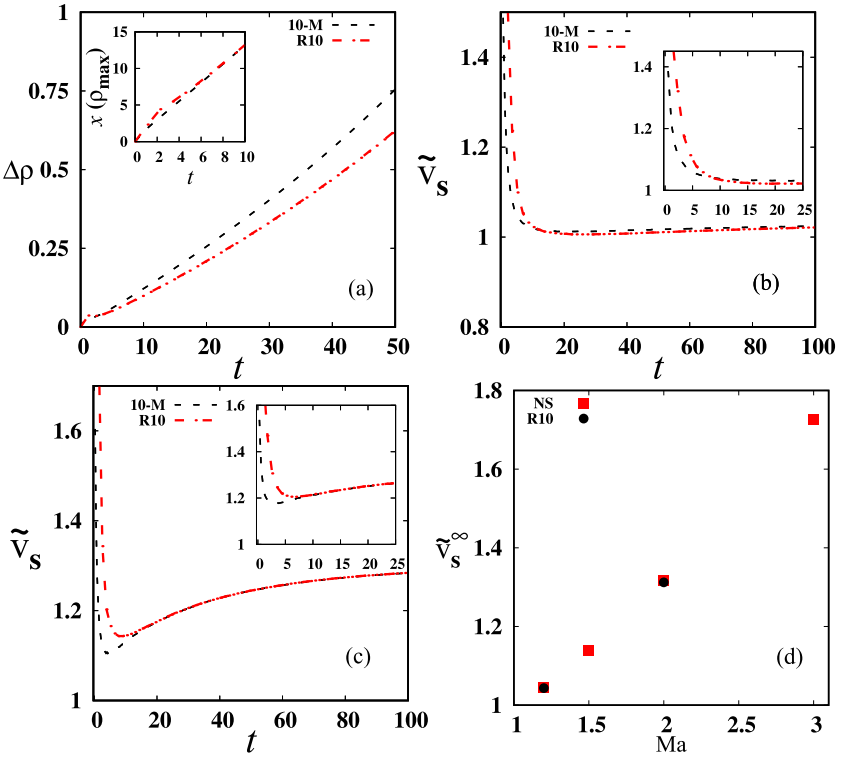

FIG. 8. (a) Temporal evolution of the density overshoot, $\triangle\rho \equiv (\rho_{\max} - \rho_2)$, for $\mathrm{Ma}_1 = 1.2$ with $\alpha = 0.9$; the inset shows the variation of the spatial location of $\rho_{\max}$ with time. (b, c) Evolution of normalized shock speed, $\tilde{v}_s = v_s/c$, where $v_s = x(\rho = \rho_{\max})/t$ is the speed of the density peak and $c = \sqrt{\gamma\theta_1}$ is the adiabatic sound speed, for $\alpha = 0.9$ (main panel) and $\alpha = 0.7$ (inset) with (b) $\mathrm{Ma}_1 = 1.2$ and (c) $\mathrm{Ma}_1 = 2$. (d) Variation of asymptotic shock speed at large times $[\tilde{v}_s^\infty \equiv \tilde{v}_s(t \to \infty)]$ with initial upstream Mach number; the circles and squares denote data from R10 and Navier-Stokes [11] model, respectively.

The temporal variations of v_s for $\mathrm{Ma}_1 = 1.2$ and $\mathrm{Ma}_1 = 2$ are displayed in Figs. 8(b) and 8(c), respectively; the restitution coefficient is set to $\alpha = 0.9$ (main panel) and $\alpha = 0.7$ (inset). It is seen that the normalized shock speed, $\tilde{v}_s = v_s/c$ [where c is the adiabatic sound speed, Eq. (51)], reaches a steady asymptotic value ($\tilde{v}_s^\infty$) at large times for both models. Comparing the inset with the main panel in Figs. 8(b) and 8(c), we find that $\tilde{v}_s^\infty$ does not seem to depend on the restitution coefficient. Figure 8(d) confirms that $\tilde{v}_s^\infty \equiv \tilde{v}_s(t \to \infty)$ increases with increasing upstream Mach number Ma_1. Overall, we conclude from Fig. 8 that the density peak travels with a steady constant speed at sufficiently late times; this conclusion holds for the Navier-Stokes model [11] too and is similar to that found for the piston-driven shock waves [59].

For an undriven granular gas with initial temperature $\theta(0)$, the hydrodynamic equations admit a spatially homogeneous solution $[\nabla(\rho, \boldsymbol{u}, \theta) = 0]$ with a time-dependent temperature $[\theta(x,t) \equiv \theta(t)]$ such that the gas cools according to Haff's law [3]:

$$\theta(t) = \frac{\theta(0)}{(1 + t/\tau_H)^2}, \quad \text{where } \tau_H = \frac{3}{2nd^2\sqrt{\pi\theta(0)}(1-\alpha^2)} \tag{69}$$

is the relaxation time. Equation (69) represents the well-known "homogeneous cooling state" (HCS) of a granular gas, and the derivation of Eq. (69) for different moment models are presented in Appendix E. The departure from Eq. (69) occurs when the system becomes inhomogeneous with cluster formation, called the "inhomogeneous cooling state" (ICS [60]). Note that in HCS the

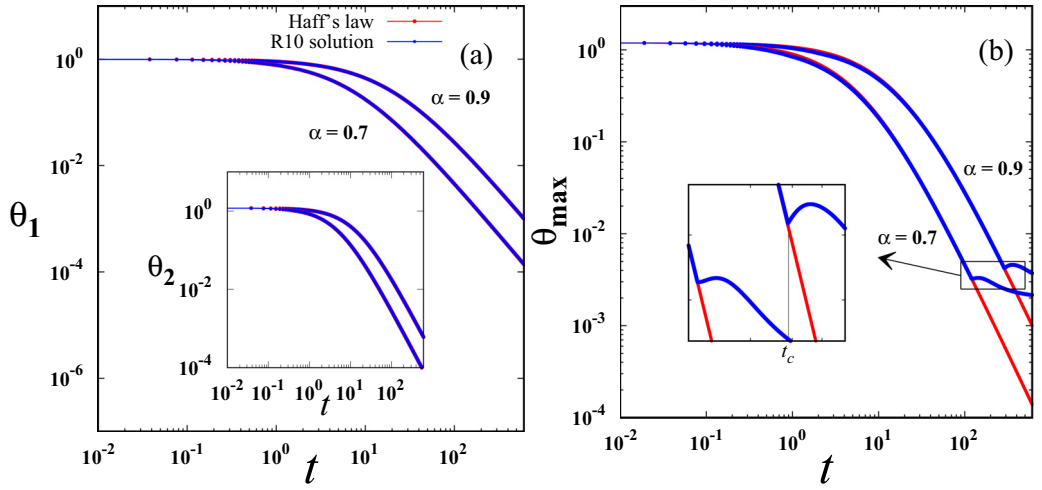

FIG. 9. Comparison of Haff's law (red curve) with the numerical solution of R10 equations for $\mathrm{Ma}_1 = 1.2$: (a) upstream temperature θ_1 (main panel), downstream temperature θ_2 (inset), and (b) maximum temperature within the shock layer $\theta_{\max}$.

density and velocities are constant in time, and hence for comparisons with Haff's law, we fix the density to be constant by taking the upstream reference density. Recall from Figs. 6(b) and 6(e) that the temperatures at the upstream [$\theta_1 \equiv \theta(x = -L/2)$] and downstream [$\theta_2 \equiv \theta(x = L/2)$] ends decay as time progresses. The temporal evolutions of θ_1 and θ_2 are compared with Eq. (69) in the main panel and inset of Fig. 9(a), respectively, for $\mathrm{Ma}_1 = 1.2$; the analogous plots for $\mathrm{Ma}_1 = 2$ are shown in Fig. 10(a). It is clear that both the upstream and downstream temperatures closely follow Haff's law for all α and Ma_1, implying that the upstream and downstream ends are in HCS.

The time evolution of the maximum granular temperature ($\theta_{\max}$) is shown in Figs. 9(b) and 10(b) for $\mathrm{Ma}_1 = 1.2$ and 2, respectively; while Fig. 9(b) shows data for $\alpha = 0.9$ (upper curve) and 0.7 (lower curve), and Fig. 10(b) displays results for $\alpha = 0.9$ only; Haff's solution, Eq. (69) [corresponding to $\theta(0) = \theta_2$ and $\rho(0) = \rho_1$], denoted by the red line, is also superimposed for each α in both figures. For the case of a weak shock [$\mathrm{Ma}_1 = 1.2$, Fig. 9(b)], $\theta_{\max}$ is seen to follow Haff's law up to a critical time [$t = t_c \approx 250$, marked by the vertical black line in the inset of Fig. 9(b) for $\alpha = 0.9$] but decays much slower thereafter. For a strong shock ($\mathrm{Ma}_1 = 2$) in Fig. 10(b), however, $\theta_{\max}(t)$ decays at a faster rate, and the critical time, $t < t_c \sim 50$, is much smaller than that for $\mathrm{Ma}_1 = 1.2$ [Fig. 9(b)]. Overall, Figs. 9(b) and 10(b) confirm that the critical time (t_c) at which the shock solution $\theta_{\max}$ crosses/overtakes Haff's solution decreases with increasing both the inelasticity $(1 - \alpha)$ and the upstream Mach number Ma_1.

The departure of the maximum temperature in the shock layer, $\theta_{\max}$, from Haff's law beyond $t > t_c$ results in a "near-saturation" of $\theta_{\max}$ at large times; see the blue curve for $t > 200$ in the main panel of Fig. 10(b). This is clearer in Fig. 10(c), which displays the temperature profiles within the shock layer at three different times, $t = 150$, 200, and 300; note that the abscissa has been shifted with respect to the location of the temperature minima. Collectively, Figs. 10(b) and 10(c) confirm that the maximum of granular temperature $\theta_{\max}$ attains a quasisteady state at a sufficiently long time ($t \gg t_c$). The long-time evolution of $\theta_{\max}(t)$ is reminiscent of the temperature evolution in the inhomogeneous cooling state [60]. More specifically, a similar kind of temperature evolution such as in Figs. 9(b) and 10(b), leading to "deviation from Haff's law," has been observed in freely cooling systems [60–62] at long times.

Figures 11(a)–11(c) and 11(d)–11(f) display the density, pressure, and longitudinal stress profiles at different times for parameter values of $\mathrm{Ma}_1 = 1.2$ with $\alpha = 0.7$ and $\mathrm{Ma}_1 = 2$ with $\alpha = 0.9$,

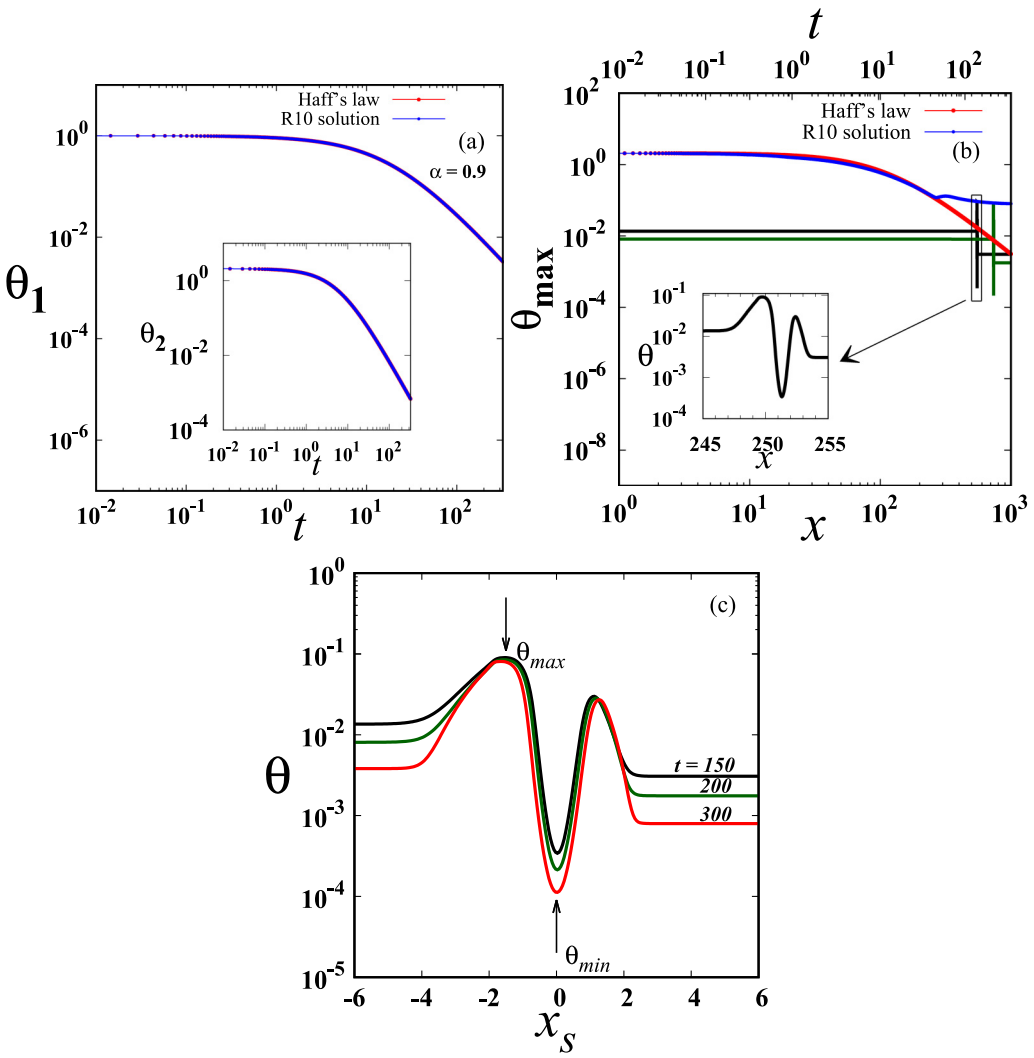

FIG. 10. (a) Comparison of Haff's law (red curve) with the numerical solution of R10 equations for $\mathrm{Ma}_1 = 2$ and $\alpha = 0.9$: upstream temperature $\theta_1(t)$ (main panel), downstream temperature $\theta_2(t)$ (inset). (b) Temporal evolution of maximum granular temperature $\theta_{\max}(t)$ (main panel, with time axis on the top). The black and green curves in panel (b) represent the spatial evolution of granular temperature $\theta(x)$ at two different times; the inset of panel (b) is a zoomed version of the black curve, containing the temperature maxima and minima. (c) Spatial evolution of granular temperature (within shock layer, such as in the inset of panel (b) at late times $t \gg t_c$; the abscissa has been shifted with respect to the location of the temperature minima.

respectively. In all panels, the abscissa, $x_s = x - x(\rho_{\max})$, has been shifted with respect to the location of the maximum density $\rho_{\max}$. The location of the density maximum (a, d) is found to coincide with that of the local minima of $p^{loc}_{\min}$ (b, e) and $\sigma^{loc}_{\min}$ (c, f) at a long enough time. This spatial location also coincides with a local minimum of the granular temperature $\theta_{\min} \equiv \theta(\rho = \rho_{\max})$; see Fig. 10(c). These overall findings also hold for other parameter values of Ma_1 and α.

Returning to the pressure profiles in Figs. 11(b) and 11(e), we note that the higher pressures on both sides of $\rho_{\max}$ create a pressure difference that drives the particles to rush in from both sides, thereby enhancing $\rho_{\max}$ with time as is evident from Figs. 11(a) and 11(d). This mechanism

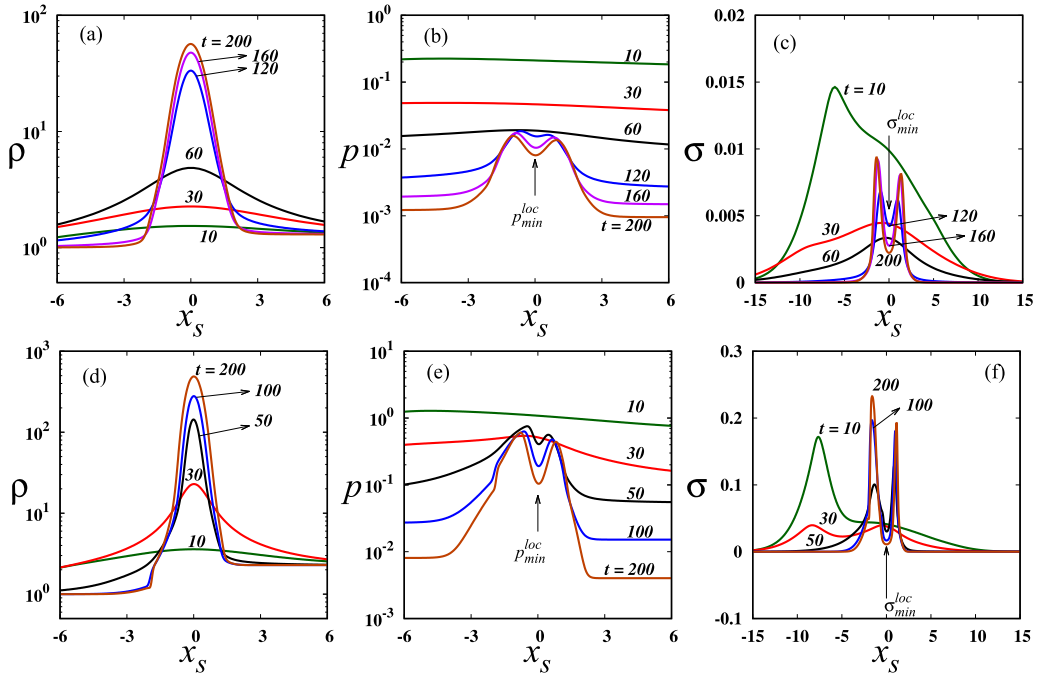

FIG. 11. Temporal evolutions of (a) density $\rho(x,t)$, (b) pressure $p(x,t)$, and (c) longitudinal stress $\sigma(x,t)$, as predicted by R10 equations, for (a), (b), (c) $\mathrm{Ma}_1 = 1.2$ and $\alpha = 0.7$ and (d), (e), (f) $\mathrm{Ma}_1 = 2$ and $\alpha = 0.9$.

is similar to the well-known *pressure instability* which drives cluster formation due to collisional cooling in both (1) undriven [18,60] and (2) driven [63–65] granular gases. Figure 12 (the green curves) confirms that $\rho_{\max}$ keeps increasing with time, and hence the density profile $\rho(x,t)$ (within shock layer) would keep changing at $t \to \infty$. This suggests, as noted previously [11], that some important physics is missing in the standard inelastic hard-sphere model: the impact velocities are likely to be lower in a relatively denser region, in comparison to those in the dilute homogeneous region and hence the collisional dissipation rate is expected be lower in the denser region. The latter point can be explained from the fact that the restitution coefficient of macroscopic particles approaches unity ($\alpha \to 1$) with decreasing impact velocity [17,19,66].

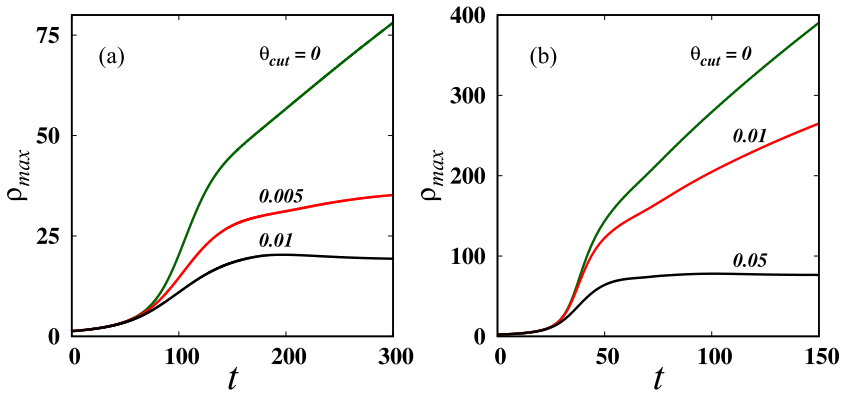

FIG. 12. Arrest of maximum density $\rho_{\max}$ via a regularization procedure for R10 equations: (a) $\mathrm{Ma}_1 = 1.2$ and $\alpha = 0.7$ and (b) $\mathrm{Ma}_1 = 2$ and $\alpha = 0.9$. For definitions of θ_{cut}, see Sec. VI C.

C. Second regularization of R10 equations

To remove the unphysical behavior of the inelastic hard-sphere model, we propose a regularization procedure that would arrest the maximum density as explained below. Note that the collisional dissipation is much lower in a denser/clustered region as the impact velocities in a granular gas are much slower in a particle-rich (clustered) region. The latter implies that when the granular system approaches a clustered state, the restitution coefficient can be taken to approach its elastic limit ($\alpha \to 1$). A related idea is that the particle collisions are of "finite" duration in a dense system that would also lead to a lower value of the inelastic dissipation. The above ideas indicates that the collisional dissipation rate (in the granular energy equation) must be modified when the granular gas enters into a clustered state. As discussed in our previous work [11], a modified expression for the collisional dissipation rate, Eqs. (10a) and (15a), can be written as

$$\mathcal{D}_{\rm reg} = \mathcal{F}(\xi)\mathcal{D}, \tag{70}$$

where $\mathcal{F}(\xi) \leqslant 1$ is called the "regularization" factor, which takes care of the above mentioned facts in a clustered state. Considering a collision model with a "cutoff" restitution coefficient, Luding and Goldshtein [62] derived an expression for

$$\mathcal{F}(\xi) = (1+\xi^2)\exp(-\xi^2), \tag{71}$$

where ξ is the ratio between the critical velocity and the local mean fluctuation velocity, which is based on the so-called T_c-model [66]. In particular,

$$\xi^2(x,t) = \frac{v_{\rm cut}^2}{v^2} \equiv \frac{\theta_{\rm cut}}{\theta(x,t)} \tag{72}$$

can be identified with the ratio between a cutoff impact energy $\theta_{\rm cut}$ (below which all collisions are treated as elastic, i.e., $\alpha = 1$) and the local fluctuation energy (or the granular temperature). We set $\mathcal{D}_{\rm reg} = 0$ whenever $\mathcal{F}[\xi(x,t)] < \mathcal{F}_{\rm cr} \ll 1$; for example, a critical/threshold value of $\mathcal{F}_{\rm cr} = 0.05$ is equivalent to $\xi_{\rm cr}^2 \approx 4.75$, and the corresponding cutoff/minimum (dimensionless) granular temperature is $\theta_{\rm min} \approx 0.21\theta_{\rm cut}$, below which the particle collisions are considered to be colliding elastically.

We have solved the R10 model [Eqs. (47a)–(47d)] for the same one-dimensional shock-wave problem, with the dissipation rate being given by Eqs. (70) and (71) and further assuming that other transport coefficients (μ, p, κ, and κ_h) remain unchanged; different values of $\theta_{\rm cut}$ have been considered in computations. The numerical results on the maximum density are shown in Figs. 12(a) and 12(b) for two values of the upstream Mach number Ma_1 and the restitution coefficient α. It is clear from Figs. 12(a) and 12(b) that the continual increase of $\rho_{\rm max}$ can indeed be inhibited after some time. The larger the value of $\theta_{\rm cut}$, the smaller the time to reach the arrested state of $\rho_{\rm max}$. For the granular shock-wave problem, the arrested density can be tied with the random-packing limit; this indicates a gas-solid-like transition as pointed out in the work of Kamenetsky *et al.* [59] for piston-driven granular shock waves. Ideally, the transport coefficients for a dense granular gas should be employed to address the above gas-solid transition in the framework of the present regularization factor given in Eq. (71); the related issues can be taken up in a future work.

VII. CONCLUSIONS AND OUTLOOK

The derivation of the "regularized" versions of 14-, 13-, and 10-moment equations (dubbed "R14," "R13," and "R10" equations) for a dilute granular gas was presented following the Chapman-Enskog-like "order-of-magnitude" method of Ref. [35]; these equations contain additional higher-order gradient terms that help to produce continuous/smooth shock solutions at all Mach numbers studied. Subsequently, Navier-Stokes-Fourier (NSF) equations were obtained via the regularization of Euler equations (which are hyperbolic and admit discontinuous shock solutions) by implementing the Maxwell-iteration procedure on (1) 13-field and (2) 14-field variables. It was shown that there is

a difference between NSF equations obtained from these two approaches: while the heat flux vector is proportional only to the temperature gradient in the first approach (i.e., the Fourier law), in the second approach the heat flux is found to be proportional to the temperature gradient as well as to the density gradient, leading to the generic "non-Fourier" law that holds in a granular gas.

In order to clarify the advantage of the regularized balance equations, the R10 equations were solved for the Riemann problem of both molecular and granular gases. Based on a comparison of results between the 10-moment and R10-moment equations, it was found that (1) while the 10-moment model fails to produce continuous shock structures beyond an upstream Mach number of $\mathrm{Ma}_1 = 1.34$, the R10 model predicts continuous and smooth shocks beyond the critical Mach number of $\mathrm{Ma}_1 = 1.34$, (2) all profiles of hydrodynamic fields predicted by the 10-moment model are steepened into a discontinuity (at $\mathrm{Ma}_1 > 1.34$) on the upstream part of the shock but this unwanted feature is not seen in the case of the profiles predicted by the R10 model, (3) the profiles predicted by the R10-moment model are less diffusive at the downstream end than at the upstream end and, last for a granular gas, (5) both R10 and 10-moment models predict asymmetric density and temperature profiles, with the maxima of both density and temperature occurring within the shock layer, and the profiles are found to be smooth for the regularized model at all Mach numbers.

Due to the collisional dissipation, the Riemann problem of a granular shock is unsteady; in particular, the density within the shock layer increases with time. The latter has been tied to an inherent deficiency of the inelastic hard-sphere model [66] since the collisions are unlikely to be binary and instantaneous in a dense/clustered system. The underlying idea is that the amount of collisional dissipation decreases in the dense limit due to (1) the finite duration of the collision process and/or (2) the reduced impact velocity of collisions which, in turn, implies the restitution coefficient approaching the limit of elastic collisions ($\alpha \to 1$). The above idea has been implemented by introducing a "regularization" factor $\mathcal{F}(\xi)$ [11,62] into the collisional dissipation term (Sec. VI C). We showed that the "second" regularization helps in arresting the continual density increase within the shock layer. It must be noted that this second regularization would be required even if we incorporate higher-order gradient terms [22,26,67] in the expression of the collisional dissipation rate since $\mathcal{D} \propto (1-\alpha^2)$ holds at any order. The effect of the above regularization factor on other transport coefficients, along with a detailed numerical analyses of granular shock waves, can be taken up in a future work. From the viewpoint of practical applications, it would be interesting to analyze the propagation of normal and oblique shock waves in a "dense" granular gas with appropriate higher-order constitutive models [26,49–52] as well as the related boundary effects [4,5,68].

ACKNOWLEDGMENTS

M.H.L.R. greatfully acknowledges support via a project assistantship (Project No. DAE/MA/4365) and a postdoctoral fellowship funded by JNCASR. He also acknowledges partial support from the UK's Engineering and Physical Sciences Research Council (EPSRC) under Grant No. EP/R008027/1 and a Ph.D. fellowship from JNCASR.

APPENDIX A: CRITICAL MACH NUMBER ANALYSIS

We consider the 10-moment system for a planar shock moving at a constant speed. Since the shock is stationary in a reference frame which is moving with the shock speed, the time derivatives vanish. For a stationary planar shock, therefore, the 10-moment equations [Eqs. (47a)–(47d), without regularized terms] for a dilute granular gas boil down to

$$\frac{d}{dx}(\rho u) = 0, \tag{A1a}$$

$$\frac{d}{dx}(\rho u^2 + \rho\theta + \sigma) = 0, \tag{A1b}$$

$$\frac{d}{dx}(\rho u^3 + 5\rho\theta u + 2\sigma u) = -3\,\mathcal{D}, \tag{A1c}$$

$$\frac{d}{dx}\left(\frac{2}{3}\rho u^3 + \frac{4}{3}\rho\theta u + \frac{7}{3}\sigma u\right) = \sigma^s, \tag{A1d}$$

where the expressions for the energy dissipation rate $\mathcal{D}$ and the source term σ^s are given in Eqs. (48c) and (48d), respectively. The boundary conditions for the above system of ODEs are supplied by the RH relations. Solving the first two equations of Eq. (A1) and using the boundary conditions, we get

$$C_1 = \rho u = \rho_1 u_1 \quad \text{and} \quad C_2 = \rho u^2 + \rho\theta + \sigma = \left(\gamma \mathrm{Ma}_1^2 + 1\right)\rho_1\theta_1, \tag{A2}$$

where $\gamma = 5/3$ is the ratio of specific heats for a monatomic gas. Recall that $\sigma = 0$ at both upstream and downstream ends. With the help of two algebraic equations,

$$u = \frac{C_1}{\rho}, \quad \sigma = C_2 - \frac{C_1^2}{\rho} - \rho\,\theta, \tag{A3}$$

which arise from Eq. (A2), the system of ODEs in Eq. (A1) can be combined to give a coupled ODEs for $\rho(x)$ and $\theta(x)$ as

$$\frac{d\rho}{dx} = \frac{\rho^3}{3\left(\gamma \mathrm{Ma}_1^2 + 1\right)C_1\,\rho_1\,\theta_1}\left(\frac{\mathcal{D} - \sigma^s}{\rho - \rho_c}\right), \tag{A4}$$

$$\frac{d\theta}{dx} = \frac{(-2\,\mathcal{D} - \sigma^s)}{3\,C_1} + \left(\frac{2\,C_1^2 - \rho\,C_2}{3\,\rho^3}\right)\frac{d\rho}{dx}, \tag{A5}$$

where

$$\rho_c = \frac{4\gamma \mathrm{Ma}_1^2}{3\left(\gamma \mathrm{Ma}_1^2 + 1\right)}\rho_1 \tag{A6}$$

is the critical density at which the density gradient in Eq. (A4) blows up. Equation (A4) has a smooth solution which connects two end states ρ_1 and ρ_2 if the upstream density is smaller than the critical density (i.e., $\rho_1 < \rho_c$). The condition for this critical state can be obtained from $\rho_c = \rho_1$:

$$\mathrm{Ma}_1 = \sqrt{\frac{3}{\gamma}} = \frac{3}{\sqrt{5}}. \tag{A7}$$

Hence the 10-moment system admits a continuous/smooth solution up to a Mach number of $\mathrm{Ma}_1 = 3/\sqrt{5} \approx 1.34$. In other words, if the shock speed is smaller than the acoustic wave speed in the system, a smooth solution exists for the system [57]. It is noteworthy that the value of the critical Mach number as well as the critical density, Eq. (A6), does not depend on the restitution coefficient (α); this is due to the fact that the source terms (which are functions of α) do not influence the critical density; see Eq. (A4). The same analysis, extended to 13- and 14-moment equations, confirmed [48,53] that the critical Mach number increases with increasing the number of moments retained in extended hydrodynamics: $\mathrm{Ma}_{\mathrm{cr}}|_{13} = 1.65$ and $\mathrm{Ma}_{\mathrm{cr}}|_{14} = 1.763$.

The above analysis clarifies that the extended hydrodynamic equations admit continuous solutions only for a finite range of Mach number ($0 \leqslant \mathrm{Ma} < \mathrm{M}_{\mathrm{cr}}$). It is possible to push the critical Mach number to infinity by retaining an infinite number of moments, thereby obtaining continuous solutions for the whole range of the Mach number, which is equivalent to solving the original Boltzmann equation. It should be noted that the continuous solution exists at any Mach number for the Navier-Stokes model; this is due to fact that the NS-equations are regularized version of Euler equations, with the latter being hyperbolic and hence admits discontinuous shock solutions as discussed in Sec. II.C 1. The connection between Euler and NS equations is established in Appendix B.

APPENDIX B: GRANULAR NAVIER-STOKES EQUATIONS FROM 14-MOMENT THEORY VIA REGULARIZATION

As discussed in Sec. III, the same regularization procedure [31,54] can be used to derive hydrodynamic equations at the Navier-Stokes (NS) order, along with related constitutive relations. We shall show that the resulting granular NS equations can be considered as a regularization of the five-moment equations, better known as Euler equations. For illustrative purposes, we start with the 14-moment equations, although the same can be achieved by starting with Grad's 13-moment theory; only the resulting transport coefficients differ slightly as we demonstrate below.

From the 14-moment theory, let us consider and rewrite the transport equations for σ_{ij}, q_i and Δ:

$$\mathcal{L}\sigma_{ij} = -\epsilon^{-1}\frac{A_6}{\tau_r}\,\sigma_{ij}, \quad \mathcal{L}q_i = -\epsilon^{-1}\frac{A_7}{\tau_r}\,q_i, \quad \mathcal{L}\Delta = -\epsilon^{-1}\frac{A_8}{\tau_r}\,[A_9\,\Delta - A_{10}]\,\rho\,\theta^2, \tag{B1}$$

where we introduced a small parameter ε on the right-hand side of each equation (B1) as a first step in the regularization process. The expressions for $\mathcal{L}\sigma_{ij}$, $\mathcal{L}q_i$, and $\mathcal{L}\Delta$ are given by

$$\mathcal{L}\sigma_{ij} \equiv \frac{\partial\sigma_{ij}}{\partial t} + \frac{\partial(\sigma_{ik}u_k)}{\partial x_k} + \frac{4}{5}\frac{\partial q_{\langle i}}{\partial x_{j\rangle}} + \frac{\partial\mathcal{Q}_{ijk}}{\partial x_k} + 2\,p\,\frac{\partial u_{\langle i}}{\partial x_{j\rangle}} + 2\,\sigma_{k\langle i}\frac{\partial u_{j\rangle}}{\partial x_k}, \tag{B2}$$

$$\mathcal{L}q_i \equiv \frac{\partial q_i}{\partial t} + \frac{\partial(q_iu_j)}{\partial x_j} - \frac{5}{2}\theta\left(\rho\frac{\partial\theta}{\partial x_i} + \theta\frac{\partial\rho}{\partial x_i} + \frac{\partial\sigma_{ij}}{\partial x_j}\right) - \frac{\sigma_{ij}}{\rho}\left(\rho\,\frac{\partial\theta}{\partial x_j} + \theta\,\frac{\partial\rho}{\partial x_j} + \frac{\partial\sigma_{jk}}{\partial x_k}\right)$$
$$+ \frac{1}{2}\frac{\partial\mathcal{R}_{ij}}{\partial x_j} + \frac{1}{6}\frac{\partial\mathcal{R}}{\partial x_i} + \frac{7}{5}\,q_j\frac{\partial u_i}{\partial x_j} + \frac{2}{5}\,q_i\frac{\partial u_j}{\partial x_j} + \frac{2}{5}\,q_k\frac{\partial u_k}{\partial x_i} + \mathcal{Q}_{ijk}\frac{\partial u_j}{\partial x_k}, \tag{B3}$$

$$\mathcal{L}\Delta \equiv 15\,\rho\,\theta^2\left(\frac{\partial\Delta}{\partial t} + u_i\,\frac{\partial\Delta}{\partial x_i}\right) - 20\,(1+\Delta)\,\theta\left(\frac{\partial q_i}{\partial x_i} + \sigma_{ij}\frac{\partial u_i}{\partial x_j}\right) + \frac{\partial\mathcal{S}_i}{\partial x_i} + 4\,\mathcal{R}_{ij}\,\frac{\partial u_i}{\partial x_j}$$
$$- 8\,q_i\,\frac{\partial\theta}{\partial x_i} - \frac{8}{\rho}\,q_i\left(\frac{\partial\sigma_{ij}}{\partial x_j} + \theta\,\frac{\partial\rho}{\partial x_i}\right), \tag{B4}$$

and the expressions for constants A_i are

$$A_6 = \frac{4}{5}(1+\alpha)(3-\alpha)\left[1 - \frac{\Delta}{32}\right], \quad A_7 = \frac{1}{15}(1+\alpha)\left[49 - 33\alpha + (19-3\alpha)\frac{\Delta}{32}\right], \tag{B5}$$

$$A_8 = 4(1+\alpha), \quad A_9 = \frac{1}{16}\left[30\alpha^2(1-\alpha) - 17\alpha + 81\right], \quad A_{10} = (1-\alpha)(1-2\alpha^2). \tag{B6}$$

1. Euler equations: Leading-order approximation

The ansatz of timescale separation of higher-order fields,

$$\sigma_{ij} = \sigma_{ij}^{(0)} + \varepsilon\,\sigma_{ij}^{(1)} + \cdots, \quad q_i = q_i^{(0)} + \varepsilon\,q_i^{(1)} + \cdots, \quad \Delta = \Delta^{(0)} + \varepsilon\,\Delta^{(1)} + \cdots, \tag{B7}$$

is then substituted into Eq. (B1), and the terms of the same order in ε are compared. It is easy to verify that the leading-order approximation for σ_{ij}, q_i, and Δ, which results from balancing the terms of order $O(\varepsilon^{-1})$ in Eq. (B1), yields

$$\sigma_{ij}^{(0)} = 0, \quad q_i^{(0)} = 0, \quad \text{and} \quad \Delta^{(0)} = 0. \tag{B8}$$

Substituting these values into the 14-moment equations yields the well-known Euler equations for a granular gas:

$$\frac{\partial \rho}{\partial t} + \frac{\partial (\rho\, u_i)}{\partial x_i} = 0, \tag{B9a}$$

$$\frac{\partial (\rho\, u_i)}{\partial t} + \frac{\partial (\rho\, u_i\, u_j)}{\partial x_j} + \frac{\partial p}{\partial x_i} = 0, \tag{B9b}$$

$$\rho\left(\frac{\partial \theta}{\partial t} + u_i\, \frac{\partial \theta}{\partial x_i}\right) + \frac{2}{3} p \frac{\partial u_i}{\partial x_i} = -\mathcal{D}_E, \tag{B9c}$$

where the equation of state is $p = \rho\theta$ and the collisional dissipation rate is

$$\mathcal{D}_E = \frac{4\sqrt{\pi}}{3} n d^2 (1-\alpha^2) \rho \theta^{3/2}. \tag{B10}$$

In principle the above approach is similar to the textbook method [32] of deriving Euler/Navier-Stokes equations from the Boltzmann equation. For example, Euler equations can be obtained by multiplying the Boltzmann equation taking $\psi = m\{1, v_i, \frac{1}{3}C^2\}$ and subsequently integrating the resulting equations over the velocity space; so the hydrodynamic variables under consideration are $(\rho,\ \rho\, u_i,\ \theta)$, and the relevant moment equations are the mass conservation law (7a), momentum conservation law (7b), and the balance equation of energy (7c). The standard Chapman-Enskog expansion then shows that the distribution function at the Euler level is the Maxwellian distribution, $f|_5 = f^M$, which yields the following constitutive relations for the stress deviator and the heat flux:

$$\sigma_{ij|5} = 0, \quad q_{i|5} = 0, \tag{B11}$$

and the resulting field equations are the same as Eq. (B9).

2. Navier-Stokes equations from the regularization of Euler equations

Balancing the terms of order $O(\varepsilon^0)$ in Eq. (B1), we obtain the equations at the first-order approximation:

$$[\mathcal{L}\sigma_{ij}]_{f_{14}} = -\frac{A_6}{\tau_r}\sigma_{ij}^{(1)}, \quad [\mathcal{L}q_i\,]_{f_{14}} = -\frac{A_7}{\tau_r} q_i^{(1)}, \quad [\mathcal{L}\Delta]_{f_{14}} = -\frac{A_8}{\tau_r}[A_9\Delta^{(1)} - A_{10}]\rho\theta^2, \tag{B12}$$

where the notation $[\cdot]_{f_{14}}$ implies that all terms are to be evaluated with the 14-moment distribution function f_{14}, which is given by Eq. (13). For example, the higher-order moments in Eq. (B12) are found to be

$$\mathcal{Q}_{ijk|14} = 0, \quad \mathcal{R}_{ij|14} = 7\,\theta\,\sigma_{ij}, \quad S_{i|14} = 28\,\theta\, q_i, \quad \mathcal{R}|_{14} = 15\,\rho\,\theta^2(1+\Delta). \tag{B13}$$

By substituting Eq. (B13) into Eq. (B12) and evaluating remaining terms inside $[\cdot]_{f_{14}}$ and subsequently equating the terms of order $O(\varepsilon^0)$ in each equation, (B12) yields

$$\sigma_{ij}^{(1)} = -\frac{2\,p\,\tau_r}{A_6}\,\frac{\partial u_{\langle i}}{\partial x_{j\rangle}}, \tag{B14a}$$

$$q_i^{(1)} = -\frac{5\,\tau_r}{2\,A_7}\left[\rho\,\theta\,\frac{\partial \theta}{\partial x_i} + 2\,\rho\,\theta\,\Delta^{(1)}\,\frac{\partial \theta}{\partial x_i} + \theta^2\ \Delta^{(1)}\,\frac{\partial \rho}{\partial x_i} + \rho\,\theta^2\,\frac{\partial \Delta^{(1)}}{\partial x_i}\right], \tag{B14b}$$

$$\Delta^{(1)} = \frac{A_{10}}{A_9} = \frac{16\,(1-\alpha)\,(1-2\,\alpha^2)}{[30\,\alpha^2\,(1-\alpha) - 17\,\alpha + 81]} \equiv \Delta. \tag{B14c}$$

At this level of approximation, the contracted fourth-moment Δ is spatially uniform and is a function of α only. Therefore, the constitutive relations for the deviatoric stress and heat flux readily

follows from the first two equations of Eq. (B14):

$$\sigma_{ij} = \sigma_{ij}^{(1)} = -2\,\mu\,\frac{\partial u_{\langle i}}{\partial x_{j\rangle}} \quad \text{and} \quad q_i = q_i^{(1)} = -\kappa\,\frac{\partial \theta}{\partial x_i} - \kappa_h\,\frac{\partial \rho}{\partial x_i}, \tag{B15}$$

where μ, κ, and κ_h denote the shear viscosity, thermal conductivity, and Dufour conductivity, respectively, given by

$$\mu = \frac{5}{4}\,\frac{m}{d^2}\sqrt{\frac{\theta}{\pi}}\,\frac{1}{(1+\alpha)(3-\alpha)\left[1-\frac{\Delta}{32}\right]}, \tag{B16a}$$

$$\kappa = \frac{75}{2}\,\frac{m}{d^2}\sqrt{\frac{\theta}{\pi}}\,\frac{1+2\,\Delta}{(1+\alpha)\left[49-33\,\alpha+(19-3\,\alpha)\,\frac{\Delta}{32}\right]}, \tag{B16b}$$

$$\kappa_h = \frac{75}{2\rho}\,\frac{m}{d^2}\,\theta\sqrt{\frac{\theta}{\pi}}\,\frac{\Delta}{(1+\alpha)\left[49-33\,\alpha+(19-3\alpha)\,\frac{\Delta}{32}\right]}, \tag{B16c}$$

$$\mathcal{D}_{NS} = \mathcal{D}_E\left(1+\frac{3}{16}\Delta\right). \tag{B16d}$$

These expressions for μ, κ, and κ_h coincide with the expressions of Refs. [25] and [40]. It is noteworthy that the heat flux vector, Eq. (B15), is proportional to the temperature gradient and the density gradient. The latter "non-Fourier" term is called Dufour flux, and it vanishes if $\Delta = 0$.

With constitutive relations as in Eq. (B15), the regularized equations at first order are given by

$$\frac{\partial \rho}{\partial t} + \frac{\partial(\rho\,u_i)}{\partial x_i} = 0, \tag{B17a}$$

$$\frac{\partial(\rho\,u_i)}{\partial t} + \frac{\partial(\rho\,u_i\,u_j)}{\partial x_j} = -\frac{\partial}{\partial x_j}(p\delta_{ij}+\sigma_{ij}), \tag{B17b}$$

$$\rho\left(\frac{\partial \theta}{\partial t} + u_i\,\frac{\partial \theta}{\partial x_i}\right) = -\frac{2}{3}\frac{\partial q_i}{\partial x_i} - \frac{2}{3}(p\delta_{ij}+\sigma_{ij})\frac{\partial u_i}{\partial x_j} - \mathcal{D}_{\rm NS}, \tag{B17c}$$

which are nothing but the well-known Navier-Stokes (NS) equations. While the Euler equations are hyperbolic and admit discontinuous shock solutions, the NS equations do not allow discontinuous shock solutions due to the presence of viscous diffusion. Therefore, the NS equations (B17) can be considered as the "regularized" version of Euler equations, or, simply the R5-moment equations (i.e., regularized five-field theory).

We remark here that, instead of the 14-moment equations, had we started with the 13-moment theory, the resulting NS-order equations (B17) would follow from the same regularization procedure, but only the expressions for μ, κ, and κ_h are slightly different:

$$\mu = \frac{5}{4}\,\frac{m}{d^2}\sqrt{\frac{\theta}{\pi}}\,\frac{1}{(1+\alpha)(3-\alpha)}, \quad \kappa = \frac{75}{2}\,\frac{m}{d^2}\sqrt{\frac{\theta}{\pi}}\,\frac{1}{(1+\alpha)\,(49-33\,\alpha)}, \quad \kappa_h = 0, \tag{B18}$$

for which the contracted fourth moment is $\Delta = 0$. This constitutes the main difference between the NS equations obtained from 14- and 13-moment theories.

APPENDIX C: PARTIAL-DIFFERENTIAL EQUATIONS IN EQ. (28)

The expressions for $\mathcal{L}\tilde{\mathcal{Q}}_{ijk}$, $\mathcal{L}\tilde{\mathcal{R}}_{ij}$, and $\mathcal{L}\tilde{\mathcal{S}}_i$ in Eq. (28) are given by

$$\begin{aligned}\mathcal{L}\tilde{\mathcal{Q}}_{ijk} \equiv & \frac{\partial \tilde{\mathcal{Q}}_{ijk}}{\partial t} + \frac{\partial(\tilde{\mathcal{Q}}_{ijk}\, u_l)}{\partial x_l} + \frac{\partial \mathcal{R}_{ijkl}}{\partial x_l} + \frac{3}{7}\frac{\partial \tilde{\mathcal{R}}_{\langle ij}}{\partial x_{k\rangle}} + 3\,\frac{\partial(\theta\,\sigma_{\langle ij})}{\partial x_{k\rangle}} - \frac{3}{\rho}\,\sigma_{\langle ij}\,\frac{\partial p}{\partial x_{k\rangle}} \\ & - \frac{3}{\rho}\,\sigma_{\langle ij}\,\frac{\partial \sigma_{k\rangle l}}{\partial x_l} + 3\,\tilde{\mathcal{Q}}_{l\langle ij}\,\frac{\partial u_{k\rangle}}{\partial x_l} + \frac{12}{5}\,q_{\langle i}\,\frac{\partial u_{k\rangle}}{\partial x_j}, \end{aligned} \tag{C1}$$

$$\begin{aligned}\mathcal{L}\tilde{\mathcal{R}}_{ij} \equiv & \frac{\partial \tilde{\mathcal{R}}_{ij}}{\partial t} + \frac{\partial(\tilde{\mathcal{R}}_{ij}\, u_k)}{\partial x_k} - 7\,\sigma_{ij}\left[\frac{\mathcal{D}}{\rho} + u_k\,\frac{\partial \theta}{\partial x_k} + \frac{2}{3\,\rho}\left(\rho\,\theta\,\frac{\partial u_k}{\partial x_k} + \sigma_{kl}\frac{\partial u_k}{\partial x_l} + \frac{\partial q_k}{\partial x_k}\right)\right] \\ & + 7\,\theta\left[\sigma^s_{\langle ij\rangle} - \frac{\partial(\sigma_{ij}\,u_k)}{\partial x_k} - \frac{4}{5}\frac{\partial q_{\langle i}}{\partial x_{j\rangle}} - \frac{\partial \tilde{\mathcal{Q}}_{ijk}}{\partial x_k} - 2\,p\,\frac{\partial u_{\langle i}}{\partial x_{j\rangle}} - 2\,\sigma_{k\langle i}\frac{\partial u_{j\rangle}}{\partial x_k}\right] \\ & + 7\frac{\partial(\theta\,\sigma_{ij}\,u_k)}{\partial x_k} + \frac{\partial \mathcal{N}_{ijk}}{\partial x_k} + \frac{2}{5}\frac{\partial \tilde{\mathcal{S}}_{\langle i}}{\partial x_{j\rangle}} + \frac{56}{5}\frac{\partial(\theta\, q_{\langle i})}{\partial x_{j\rangle}} + 2\,\mathcal{R}_{ijkl}\,\frac{\partial u_l}{\partial x_k} + 14\,\rho\,\theta^2\,\frac{\partial u_{\langle i}}{\partial x_{j\rangle}} \\ & + 14\,\rho\,\theta^2\,\Delta\,\frac{\partial u_{\langle i}}{\partial x_{j\rangle}} + 2\,\tilde{\mathcal{R}}_{k\langle i}\,\frac{\partial u_{j\rangle}}{\partial x_k} + 14\,\theta\,\sigma_{k\langle i}\frac{\partial u_{j\rangle}}{\partial x_k} + \frac{4}{5}\tilde{\mathcal{R}}_{k\langle i}\,\frac{\partial u_k}{\partial x_{j\rangle}} + \frac{28}{5}\,\theta\,\sigma_{k\langle i}\,\frac{\partial u_k}{\partial x_{j\rangle}} \\ & + \frac{6}{7}\tilde{\mathcal{R}}_{\langle ij}\,\frac{\partial u_{k\rangle}}{\partial x_k} + 6\,\theta\,\sigma_{\langle ij}\,\frac{\partial u_{k\rangle}}{\partial x_k} - \frac{2}{\rho}\,\tilde{\mathcal{Q}}_{ijk}\,\frac{\partial p_{kl}}{\partial x_l} - \frac{28}{5\,\rho}\,q_{\langle i}\,\frac{\partial p_{j\rangle k}}{\partial x_k}, \end{aligned} \tag{C2}$$

$$\begin{aligned}\mathcal{L}\tilde{\mathcal{S}}_i \equiv & \frac{\partial \tilde{\mathcal{S}}_i}{\partial t} + \frac{\partial(\tilde{\mathcal{S}}_i\, u_j)}{\partial x_j} - 28\,q_i\left[\frac{\mathcal{D}}{\rho} + u_j\,\frac{\partial \theta}{\partial x_j} + \frac{2}{3\,\rho}\left(\rho\,\theta\,\frac{\partial u_j}{\partial x_j} + \sigma_{jk}\frac{\partial u_j}{\partial x_k} + \frac{\partial q_j}{\partial x_j}\right)\right] begin \\ & - 28\,\theta\left\{-q^s_i + \frac{\partial(q_i\,u_j)}{\partial x_j} + \frac{1}{2}\frac{\partial \tilde{\mathcal{R}}_{ij}}{\partial x_j} + \frac{7}{2}\frac{\partial(\theta\,\sigma_{ij})}{\partial x_j} + \frac{5}{2}\,\frac{\partial[\rho\,\theta^2\,(1+\Delta)]}{\partial x_i}\right. \\ & - \frac{5}{2}\,\theta\left(\rho\,\frac{\partial \theta}{\partial x_i} + \theta\,\frac{\partial \rho}{\partial x_i} + \frac{\partial \sigma_{ij}}{\partial x_j}\right) - \frac{\sigma_{ij}}{\rho}\left(\rho\,\frac{\partial \theta}{\partial x_j} + \theta\,\frac{\partial \rho}{\partial x_j} + \frac{\partial \sigma_{jk}}{\partial x_k}\right) + \frac{7}{5}\,q_j\,\frac{\partial u_i}{\partial x_j} \\ & \left. + \frac{2}{5}\,q_i\,\frac{\partial u_j}{\partial x_j} + \frac{2}{5}\,q_k\,\frac{\partial u_k}{\partial x_i} + \tilde{\mathcal{Q}}_{ijk}\,\frac{\partial u_j}{\partial x_k}\right\} + 28\,\frac{\partial(\theta\,q_i\,u_j)}{\partial x_j} + \frac{\partial \mathcal{M}^{(6)}_{ij}}{\partial x_j} + 4\,\mathcal{N}_{ijk}\,\frac{\partial u_k}{\partial x_j} \\ & - \frac{4}{\rho}\tilde{\mathcal{R}}_{ij}\,\frac{\partial p_{jk}}{\partial x_k} - \frac{28}{\rho}\theta\,\sigma_{ij}\,\frac{\partial p_{jk}}{\partial x_k} - 35\,\theta^2\,(1+\Delta)\,\frac{\partial p_{ij}}{\partial x_j} + \frac{4}{5}\left(\tilde{\mathcal{S}}_i\,\frac{\partial u_j}{\partial x_j} + \tilde{\mathcal{S}}_j\,\frac{\partial u_j}{\partial x_i}\right) \\ & + \frac{9}{5}\,\tilde{\mathcal{S}}_j\,\frac{\partial u_i}{\partial x_j} + \frac{112}{5}\,\theta\left[q_i\,\frac{\partial u_j}{\partial x_j} + q_j\left(\frac{\partial u_i}{\partial x_j} + \frac{\partial u_j}{\partial x_i}\right)\right] + 28\,\theta\,q_j\,\frac{\partial u_i}{\partial x_j}. \end{aligned} \tag{C3}$$

APPENDIX D: REFERENCE VARIABLES AND THE NUMERICAL SCHEME

To nondimensionalize the independent position variable x, we look for a relevant length scale. The changes through the shock profile occur due to collisions, so the mean-free path (l) is a natural choice for the length scale. The expression for the mean-free path of a hard-sphere gas is

$$l = \frac{16\,\mu}{5\,\sqrt{2\pi}\,\rho\sqrt{\theta}}, \tag{D1}$$

where the shear viscosity coefficient μ for a hard-sphere gas is given by Eq. (B18). For present shock-wave calculations, all quantities are nondimensionalized by the "upstream" reference state quantities. The dimensionless variables are given by

$$\widehat{\rho} = \frac{\rho}{\rho_1(0)}, \quad \widehat{u} = \frac{u}{\sqrt{\theta_1(0)}}, \quad \widehat{\theta} = \frac{\theta}{\theta_1(0)}, \quad \widehat{\sigma} = \frac{\sigma}{\rho_1(0)\,\theta_1(0)}, \tag{D2a}$$

$$\widehat{q} = \frac{q}{\rho_1(0)\,\theta_1(0)\,\sqrt{\theta_1(0)}}, \quad \widehat{x} = \frac{x}{l_1}, \quad \widehat{t} = \frac{t\sqrt{\theta_1(0)}}{l_1}. \tag{D2b}$$

For simplicity we remove the hat from the dimensionless quantities.

The one-dimensional reduced balance equations (47a)–(47d) in dimensionless form can be expressed in operator form

$$\frac{\partial \mathbf{U}}{\partial t} + \frac{\partial \mathbf{F}(\mathbf{U})}{\partial x} = \mathbf{G}(\mathbf{U}), \tag{D3}$$

where $\mathbf{U}$ is the vector of variables, $\mathbf{F}(\mathbf{U})$ is the vector of flux, and $\mathbf{G}(\mathbf{U})$ is the vector of source terms. The explicit forms of $\mathbf{U}$, $\mathbf{F}(\mathbf{U})$ and $\mathbf{G}(\mathbf{U})$ for R10-moment model are given by

$$\mathbf{U} = \begin{pmatrix} \rho \\ \rho\, u \\ \rho u^2 + 3\rho\theta \\ \frac{2}{3}\rho u^2 + \sigma \end{pmatrix}, \quad \mathbf{F}(\mathbf{U}) = \begin{pmatrix} \rho\, u \\ \rho u^2 + \rho\theta + \sigma \\ \rho u^3 + 5\rho\theta u + 2\sigma u \\ \frac{2}{3}\rho u^3 + \frac{4}{3}\rho\theta u + \frac{7}{3}\sigma u \end{pmatrix}, \quad \mathbf{G}(\mathbf{U}) = \begin{pmatrix} 0 \\ 0 \\ -3\,\mathcal{D} - 2\frac{\partial q}{\partial x} \\ \sigma^s - \frac{8}{15}\frac{\partial q}{\partial x} - \frac{\partial \mathcal{Q}}{\partial x} \end{pmatrix}. \tag{D4}$$

The solution of Eq. (D3) along with Rankine-Hugoniot conditions, Eq. (52a), is obtained by implementing the relaxation scheme of Delis and Katsaounis [55,56], which is briefly described below. For the inhomogeneous system (D3), the equivalent relaxation system is given by

$$\frac{\partial \mathbf{U}}{\partial t} + \frac{\partial \mathbf{V}}{\partial x} = \mathbf{G}(\mathbf{U}), \tag{D5}$$

$$\frac{\partial \mathbf{V}}{\partial t} + \mathbf{A}\frac{\partial \mathbf{U}}{\partial x} = -\frac{1}{\epsilon}[\mathbf{V} - \mathbf{F}(\mathbf{U})], \tag{D6}$$

where $\mathbf{U} \in \mathbf{R^n}$, $\mathbf{V} \in \mathbf{R^n}$, $x \in \mathbf{R}$, $t \in \mathbf{R}^+$, and $\epsilon \ll 1$ is the relaxation rate. Note that the numerical scheme of Refs. [55,56] is a variant of that proposed in Ref. [69] but incorporates the source terms in the relaxation step; for a comparative performance of two numerical methods, see Ref. [48,70,71]. In any case, the original inhomogeneous system (D3) has been replaced by a linear hyperbolic system, Eqs. (D5) and (D6), with a relaxation source term. Putting the relaxation limit $\epsilon \to 0$ into the hyperbolic part of the relaxation system Eq. (D6), we obtain the local equilibrium solution $\mathbf{V} = \mathbf{F}(\mathbf{U})$. For the convergence of the relaxation system, Eqs. (D5) and (D6), it is necessary that $\mathbf{F}'(\mathbf{U}) - \mathbf{A} \leqslant \mathbf{0}$ for all $\mathbf{U}$, where $\mathbf{F}'(\mathbf{U})$ is the Jacobian of flux $\mathbf{F}(\mathbf{U})$. The structure of $\mathbf{A}$ is taken to be of the form [55,56]

$$\mathbf{A} = \text{diag}\{a_1, a_2, \cdots, a_n\}, \quad \text{with } a_m > 0 \quad (1 \leqslant m \leqslant n). \tag{D7}$$

Since the Jacobian $\mathbf{F}'(\mathbf{U})$ constitutes a complete eigensystem $\{\lambda_1, \lambda_2, \ldots, \lambda_n\}$, one can either take $a_i = sup|\lambda_i|$, or, $a_1 = a_2 = \cdots = a_n = \max(sup|\lambda_1|, sup|\lambda_2|, \ldots, sup|\lambda_n|)$ for all t and x; both choices satisfy $-\sqrt{a_m} \leqslant \lambda_m \leqslant \sqrt{a_m}$ [55,56] for all $\mathbf{U}$ and $1 \leqslant m \leqslant n$. In this work, we choose

$$a_1 = a_2 = \cdots = a_n = \max(\sup|\lambda_1|, \sup|\lambda_2|, \ldots, \sup|\lambda_n|) \quad \forall \quad (x, t) \tag{D8}$$

to construct the diagonal matrix $\mathbf{A}$ in Eq. (D7).

The spatially uniform grids with a grid size Δx are used, along with a uniform time step of Δt; the spatial (Δx) and temporal (Δt) steps are related via the Courant-Friedrichs-Lewy (CFL) condition, $\mathcal{C} = \max(a_i\, \Delta t/\Delta x) < 1$. The relaxation rate ϵ plays the role of numerical viscosity, so

more numerical diffusion will be added for larger values of ϵ. Hence the relaxation rate ϵ must be very small compared to both the time step and the spatial step (i.e., $\epsilon \ll \Delta t$ and $\epsilon \ll \Delta x$); in all numerical simulations the relaxation rate ϵ is taken to be 10^{-8} as this gives converged results for the present shock-wave problem of molecular and granular gases. Other details of the present numerical scheme can be found in Refs. [48,55,56].

APPENDIX E: HAFF'S LAW FROM MOMENT MODELS: HOMOGENEOUS COOLING STATE (HCS)

Here we analyze the homogeneous cooling state (HCS) [3,18,19,60] of a granular gas, based on the 10- and 14-moment equations. Note that the HCS refers to a spatially homogeneous state with no macroscopic velocity, with possible time dependence of underlying hydrodynamic fields. It was originally analyzed by Haff [3] who showed that the granular temperature in HCS decays quadratically with time [$T(t) \sim t^{-2}$], known as Haff's law. The effect of higher-order fields on Haff's law is analyzed in the following sections.

1. Haff's law from 14-moment model

For a spatially homogeneous system, all the basic field variables depend only on time. Hence, for the spatially homogeneous solution, the 14-moment model reduces to the following system of six equations in one dimension for the density (ρ), velocity (u), granular temperature (θ), longitudinal stress (σ), heat flux (q), and fourth moment or cumulant (Δ):

$$\frac{d\rho}{dt} = 0 = \frac{du}{dt}, \tag{E1a}$$

$$\frac{d\theta}{dt} = = -\frac{8\sqrt{2}}{3\sqrt{\pi}}\frac{(1-\alpha)}{(3-\alpha)}\sqrt{\theta}\left[1-\frac{\Delta}{32}\right]\rho\,\theta, \tag{E1b}$$

$$\frac{d\sigma}{dt} = = -\frac{8\sqrt{2}}{5\sqrt{\pi}}\sqrt{\theta}\left[1-\frac{\Delta}{32}\right]\rho\,\sigma, \tag{E1c}$$

$$\frac{dq}{dt} = -\frac{2\sqrt{2}}{15\sqrt{\pi}}\frac{\sqrt{\theta}}{(3-\alpha)}\left[49-33\alpha+(19-3\alpha)\frac{\Delta}{32}\right]\rho\,q, \tag{E1d}$$

$$\frac{d\Delta}{dt} = -\frac{\sqrt{2}}{30\sqrt{\pi}}\frac{\rho\sqrt{\theta}}{(3-\alpha)}\{16(2\alpha^2-1)(1-\alpha)+\Delta[30\alpha^2(1-\alpha)+81-17\alpha]\}. \tag{E1e}$$

Note that we retained only linear terms in Δ in Eq. (E1e). All the above equations have been made dimensionless using the reference parameters

$$\widehat{\rho} = \frac{\rho}{\rho_1}, \quad \widehat{u} = \frac{u}{\sqrt{\theta_1}}, \quad \widehat{\theta} = \frac{\theta}{\theta_1}, \quad \widehat{\theta}_s = \frac{\theta_s}{\theta_1}, \quad \widehat{q} = \frac{q}{\rho_1\theta_1\sqrt{\theta_1}}, \quad \widehat{t} = \frac{t}{\tau}, \tag{E2}$$

with

$$\tau = \frac{4}{\sqrt{2}n_1\pi d^2\sqrt{\theta_1}(1+\alpha)(3-\alpha)}, \tag{E3}$$

and the hats are removed for simplicity. From Eq. (E1a), we find that the mass density and the velocity remain constant in time, and furthermore the mass density (ρ) is taken to be one. It is clear from Eqs. (E1c)–(E1d) that the longitudinal stress and the heat flux do not evolve in time when the initial conditions for these two variables vanish. It is clear from Eq. (E1e) that the fourth moment evolves in time.

Let us consider a special case in which the fourth moment is constant in time,

$$\Delta_\infty \equiv \Delta(t \to \infty) = \frac{16(1-2\alpha^2)(1-\alpha)}{30\alpha^2(1-\alpha)+81-17\alpha} \equiv a_2, \tag{E4}$$

that follows from Eq. (E1e). Substituting the above value of Δ into Eq. (E1b) and integrating the resulting equation leads to

$$\theta(t) = \frac{\theta(t=0)}{\left\{1+\frac{4\sqrt{2}}{3\sqrt{\pi}}\frac{(1-\alpha)}{(3-\alpha)}\left[1+\frac{3(1-\alpha)(1-2\alpha^2)}{30\alpha^2(1-\alpha)+81-17\alpha}\right]\sqrt{\theta(t=0)}\,\rho(t=0)\,t\right\}^2} \equiv \frac{1}{(k_0+k_1\,t)^2}. \tag{E5}$$

The above equation can be simplified to

$$\theta(t) = \frac{1}{(k_0+k_1\,t)^2}, \tag{E6}$$

where

$$k_0 = \frac{1}{\sqrt{\theta(t=0)}} \quad \text{and} \quad k_1 = \frac{4\sqrt{2}}{3\sqrt{\pi}}\frac{(1-\alpha)}{(3-\alpha)}\left(1+\frac{3}{16}\Delta_\infty\right)\rho(0). \tag{E7}$$

Now we solve the coupled nonlinear system (E1a)–(E1e) semianalytically by treating Δ_∞ as the stationary solution for Δ. In terms of a new variable $\delta(t) = \Delta(t) - \Delta_\infty$, Eq. (E1b) can be rewritten as

$$\frac{d\delta(t)}{dt} = -\frac{\sqrt{2}}{30\sqrt{\pi}}\frac{1}{(3-\alpha)}[30\alpha^2(1-\alpha)+81-17\alpha]\,\rho\,\sqrt{\theta(t)}\,\delta(t). \tag{E8}$$

Solving this equation with the help of Eq. (E1e) we obtain

$$\delta(t) = k_0^{(k_2/k_1)}\,\delta(0)\,(k_0+k_1\,t)^{-\frac{k_2}{k_1}}, \tag{E9}$$

where

$$k_2 = \frac{\sqrt{2}}{30\sqrt{\pi}}\frac{1}{(3-\alpha)}[30\alpha^2(1-\alpha)+81-17\alpha]\,\rho. \tag{E10}$$

Substituting $\delta(t)$ into Eq. (E1b), we get

$$\frac{d\theta(t)}{dt} = -[k_3 + k_4(k_0+k_1\,t)^{-(k_2/k_1)}]\theta(t)\sqrt{\theta(t)}, \tag{E11}$$

where

$$k_3 = \frac{8\sqrt{2}}{3\sqrt{\pi}}\frac{(1-\alpha)}{(3-\alpha)}\left[1+\frac{3}{16}\Delta_\infty\right]\rho \quad \text{and} \quad k_4 = \frac{1}{\sqrt{2\pi}}\frac{(1-\alpha)}{(3-\alpha)}\,k_0^{\frac{k_2}{k_1}}\,\rho\,\delta(0). \tag{E12}$$

The solution to Eq. (E5) is

$$\theta(t) = \frac{4(k_1-k_2)^2\,(k_0+k_1\,t)^{2(k_2/k_1)}}{\left\{k_4(k_0+k_1\,t)+(k_1-k_2)\,(k_0+k_1\,t)^{(k_2/k_1)}\left[k_3\,t-\frac{k_4}{k_1-k_2}\,k_0^{1-(k_2/k_1)}+\frac{2}{\sqrt{\theta(0)}}\right]\right\}^2}. \tag{E13}$$

2. Haff's law from 10-moment model

The spatially homogeneous 10-moment model in one dimension [Eqs. (41a)–(41d)] reduces to the following system for four field variables, namely, the density (ρ), the velocity (u), the granular

temperature (θ), and the longitudinal stress (σ):

$$\frac{d\rho}{dt} = 0 = \frac{du}{dt}, \tag{E14a}$$

$$\frac{d\theta}{dt} = -\frac{8\sqrt{2}}{3\sqrt{\pi}}\frac{(1-\alpha)}{(3-\alpha)}\rho\,\theta^{\frac{3}{2}}, \tag{E14b}$$

$$\frac{d\sigma}{dt} = -\frac{8\sqrt{2}}{5\sqrt{\pi}}\sqrt{\theta}\,\rho\,\sigma. \tag{E14c}$$

The above equations have been made dimensionless by using the reference scales in Eq. (E2). The mass density and the velocity remain constant in time, which follows from Eq. (E14a). On integrating the temperature equation and using the initial condition, we arrive at Haff's law:

$$\theta(t) = \frac{\theta(t=0)}{\left[1 + \frac{4\sqrt{2}}{3\sqrt{\pi}}\frac{(1-\alpha)}{(3-\alpha)}\sqrt{\theta(t=0)}\,\rho(t=0)\,t\right]^2}. \tag{E15}$$

Note that Haff's law (E15) derived from 10-moment model and 13-moment model (not shown) coincides with the original Haff's law (69). Hence the main difference between the original Haff's law and the one derived from the 14-moment model is the presence of the factor $(1 + \frac{3}{16}a_2)$ in the denominator, where a_2 is the stationary value of the nonequilibrium part of the full contracted fourth moment (Δ_∞); see Eq. (E4).

[1] S. B. Savage and D. J. Jeffrey, The stress tensor in a granular flow at high shear rates, J. Fluid Mech. **110**, 255 (1981).

[2] J. T. Jenkins and S. B. Savage, A theory for the rapid flow of identical, smooth, nearly elastic, spherical particles, J. Fluid Mech. **130**, 187 (1983).

[3] P. K. Haff, Grain flow as a fluid mechanical phenomenon, J. Fluid Mech. **134**, 401 (1983).

[4] E. C. Rericha, C. Bizon, M. D. Shattuck, and H. L. Swinney, Shocks in Supersonic Sands, Phys. Rev. Lett. **88**, 014302 (2001).

[5] J. M. N. T. Gray, Y. C. Tai, and S. Noelle, Shock waves, dead-zones and particle-free regions in rapid granular free surface flows, J. Fluid Mech. **491**, 161 (2003).

[6] M. Alam, V. H. Arakeri, P. R. Nott, J. D. Goddard, and H. J. Herrmann, Instability-induced ordering, universal unfolding and the role of gravity in granular Couette flow, J. Fluid Mech. **523**, 277 (2005).

[7] B. Gayen and M. Alam, Orientational Correlation and Velocity Distributions in Uniform Shear Flow of a Dilute Granular Gas, Phys. Rev. Lett. **100**, 068002 (2008).

[8] J. F. Boudet, Y. Amarouchene, and H. Kellay, Shock Front Width and Structure in Supersonic Granular Flows, Phys. Rev. Lett. **101**, 254503 (2008).

[9] V. Chikkadi and M. Alam, Slip velocity and stresses in granular Poiseuille flow via event-driven simulation, Phys. Rev. E **80**, 021303 (2009).

[10] M. Alam, A. Mahajan, and D. Shivanna, On Knudsen-minimum effect and temperature bimodality in a dilute granular Poiseuille flow, J. Fluid Mech. **782**, 99 (2015).

[11] M. H. L. Reddy and M. Alam, Plane shock waves and Haff's law in a granular gas, J. Fluid Mech. **779**, R2 (2015).

[12] R. Gupta and M. Alam, Disentangling the role of athermal walls on the Knudsen paradox in molecular and granular gases, Phys. Rev. E **97**, 012912 (2018).

[13] Y. Forterre and O. Pouliquen, Flows of dense granular media, Annu. Rev. Fluid Mech. **40**, 1 (2008).

[14] K. K. Rao and P. R. Nott, *Introduction to Granular Flows* (Cambridge University Press, New York, 2008).

[15] H. M. Jaeger, S. Nagel, and R. P. Behringer, Granular solids, liquids and gases, Rev. Mod. Phys. **68**, 1259 (1996).

[16] C. S. Campbell, Rapid granular flows, Annu. Rev. Fluid Mech. **22**, 57 (1990).

[17] I. Goldhirsch, Rapid granular flows, Annu. Rev. Fluid Mech. **35**, 267 (2003).
[18] I. Goldhirsch and G. Zanetti, Clustering Instability in Dissipative Gases, Phys. Rev. Lett. **70**, 1619 (1993).
[19] T. Pöschel and S. Luding, *Granular Gases* (Springer-Verlag, Berlin, 2001).
[20] J. T. Jenkins and M. W. Richman, Kinetic theory for plane flows of a dense gas of identical, rough, inelastic, circular disks, Phys. Fluids **28**, 3485 (1985).
[21] A. Goldshtein and M. Shapiro, Mechanics of collisional motion of granular materials. Part 1. General hydrodynamic equations, J. Fluid Mech. **282**, 75 (1995).
[22] J. J. Brey, J. W. Dufty, C. S. Kim, and A. Santos, Hydrodynamics for granular flow at low density, Phys. Rev. E **58**, 4638 (1998).
[23] N. Sela and I. Goldhirsch, Hydrodynamic equations for rapid shear flows of smooth, inelastic spheres, to Burnett order, J. Fluid Mech. **361**, 41 (1998).
[24] N. V. Brilliantov and T. Pöschel, *Kinetic Theory of Granular Gases* (Oxford University Press, Oxford, 2004).
[25] V. Garzo, A. Santos, and J. M. Montanero, Modified Sonine approximation for the Navier-Stokes transport coefficients of a granular gas, Physica A **376**, 94 (2007).
[26] S. Saha and M. Alam, Non-Newtonian stress, collisional dissipation and heat flux in the shear flow of inelastic disks: A reduction via Grad's moment method, J. Fluid Mech. **757**, 251 (2014).
[27] R. Rongali and M. Alam, Higher-order effects on orientational correlation and relaxation dynamics in homogeneous cooling of a rough granular gas, Phys. Rev. E **89**, 062201 (2014).
[28] H. Grad, On the kinetic theory of rarefied gases, Commun. Pure Appl. Math. **2**, 331 (1949).
[29] I. Müller and T. Ruggeri, *Rational Extended Thermodynamics* (Springer, Berlin, 2013).
[30] H. Grad, Principles of the kinetic theory of gases, in *Handbuch der Physik*, edited by S. Flügge, Vol. XII, Sec. 26 (Springer-Verlag, Berlin, 1958).
[31] H. Struchtrup, *Macroscopic Transport Equations for Rarefied Gas Flows* (Springer, Berlin, 2005).
[32] S. Chapman and T. G. Cowling, *The Mathematical Theory of Non-Uniform Gases* (Cambridge University Press, Cambridge, 1970).
[33] C. Cercignani, *The Boltzmann Equation and its Applications* (Springer, New York, 1988).
[34] A. V. Bobylev, The Chapman-Enskog and Grad methods for solving the Boltzmann equation, Sov. Phys. Dokl. **27**, 29 (1982).
[35] H. Struchtrup, Stable transport equations for rarefied gases at high orders in the Knudsen number, Phys. Fluids **16**, 3921 (2004).
[36] H. Struchtrup and M. Torrilhon, Regularization of Grad's 13-moment equations: Derivation and linear analysis, Phys. Fluids **15**, 2668 (2003).
[37] M. Torrilhon and H. Struchtrup, Regularized 13-moment equations: Shock structure calculations and comparison to Burnett models, J. Fluid Mech. **513**, 171 (2004).
[38] A. V. Bobylev, Instabilities in the Chapman-Enskog expansion and hyperbolic Burnett equations, J. Stat. Phys. **124**, 371 (2006).
[39] M. Colangeli, I. V. Karlin, and M. Krüger, From hyperbolic regularization to exact hydrodynamics for linearized Grad's equations, Phys. Rev. E **75**, 051204 (2007).
[40] G. M. Kremer and W. Marques, Fourteen moment theory for granular gases, Kinet. Relat. Models **4**, 317 (2011).
[41] I. Müller, D. Reitebuch, and W. Weiss, Extended thermodynamics—Consistent in order of magnitude, Continuum Mech. Thermodyn. **15**, 113 (2003).
[42] P. Prasad, *Nonlinear Hyperbolic Waves in Multi-Dimensions* (Chapman & Hall, London, 2001).
[43] R. Courant and K. O. Friedrichs, *Supersonic Flows and Shock Waves* (Interscience, New York, 1948).
[44] H. Bateman, Some recent researches on the motion of fluids, Mon. Weather Rev. **43**, 163 (1915).
[45] J. M. Burgers, A mathematical model illustrating the theory of turbulence, Adv. Appl. Mech. **1**, 171 (1948).
[46] C. Truesdell and R. G. Muncaster, *Fundamentals of Maxwell's Kinetic Theory of a Simple Monatomic Gas* (Academic, New York, 1980).
[47] X. Gu and D. R. Emerson, A high-order moment approach for capturing non-equilibrium phenomena in the transition regime, J. Fluid Mech. **636**, 177 (2009).

[48] M. H. L. Reddy, Plane shock waves in granular gases and regularized moment equations, Ph.D. Thesis, GrainLab, Jawaharlal Nehru Centre for Advanced Scientific Research, India (2016).
[49] S. Saha and M. Alam, Normal stress differences, their origin and constitutive relations for a sheared granular fluid, J. Fluid Mech. **795**, 549 (2016).
[50] S. Saha and M. Alam, Revisiting ignited-quenched transition and the non-Newtonian rheology of a sheared dilute gas-solid suspension, J. Fluid Mech. **833**, 206 (2017).
[51] M. Alam, S. Saha, and R. Gupta, Unified theory for a sheared gas-solid suspension: From rapid granular suspension to its small-Stokes-number limit, J. Fluid Mech. **870**, 206 (2019).
[52] S. Saha and M. Alam, Burnett-order constitutive relations, second moment anisotropy and co-existing states in sheared dense gas-solid suspensions, J. Fluid Mech. **887**, A9 (2020).
[53] W. Weiss, Continuous shock structure in extended thermodynamics, Phys. Rev. E **52**, 5760(R) (1995).
[54] M. H. L. Reddy and M. Alam, Regularized moment equations and plane shock waves for a rarefied granular gas, Bull. Am. Phys. Soc. **61** (2016).
[55] A. I. Delis and T. Katsaounis, Relaxation schemes for the shallow water equations, Int. J. Numer. Methods Fluids **41**, 695 (2003).
[56] A. I. Delis and T. Katsaounis, Numerical solution of the two-dimensional shallow water equations by the application of relaxation methods, Appl. Math. Model **29**, 754 (2005).
[57] C. D. Levermore and W. J. Morokoff, The Gaussian moment closure for gas dynamics, SIAM J. Appl. Math. **59**, 72 (1998).
[58] M. Yu. Timokhin, Ye. A. Bondar, A. A. Kokhanchik, M. S. Ivanov, I. E. Ivanov, and I. A. Kryukov, Study of the shock wave structure by regularized Grad's set of equations, Phys. Fluids **27**, 037101 (2015).
[59] V. Kamenetsky, A. Goldshtein, M. Shapiro, and D. Degani, Evolution of a shock wave in a granular gas, Phys. Fluids **12**, 3036 (2000).
[60] S. Luding and H. J. Herrmann, Cluster growth in freely cooling granular media, Chaos **8**, 673 (1999).
[61] S. Gonzalez, A. R. Thornton, and S. Luding, Free cooling phase-diagram of hard-spheres with short-and long-range interactions, Eur. Phys. J.: Spec. Top. **223**, 2205 (2014).
[62] S. Luding and A. Goldshtein, Collisional cooling with multi-particle interactions, Granular Matter **5**, 159 (2003).
[63] M. Alam and P. R. Nott, The influence of friction on the stability of unbounded granular shear flow, J. Fluid Mech. **343**, 267 (1997).
[64] M. Alam and P. R. Nott, Stability of plane Couette flow of a granular material, J. Fluid Mech. **377**, 99 (1998).
[65] B. Gayen and M. Alam, Algebraic and exponential instabilities in a sheared micropolar granular fluid, J. Fluid Mech. **567**, 195 (2006).
[66] S. Luding and S. McNamara, How to handle the inelastic collapse of a dissipative hard-sphere gas with the T_c-model? Granular Matter **1**, 113 (1998).
[67] N. V. Brilliantov and T. Pöschel, Hydrodynamics and transport coefficients for dilute granular gases, Phys. Rev. E **67**, 061304 (2003).
[68] N. Gopan and M. Alam, Oblique shock waves in granular flows over bluff-bodies, EPJ. Web Conf. **140**, 03053 (2017).
[69] X. Jin and Z. Xin, The relaxation schemes for systems of conservation laws in arbitrary space dimensions, Commun. Pure Appl. Math. **48**, 235 (1995).
[70] M. H. L. Reddy, S. Ansumali, and M. Alam, Shock waves in a dilute granular gas, AIP Conf. Proc. **1628**, 480 (2014).
[71] M. H. L. Reddy and M. Alam, Plane shock wave structure in a dilute granular gas, AIP Conf. Proc. **1786**, 120001 (2016).